Chapter 6

Matrix Microcracking

J. A. NAIRN and S. HU

Department of Materials Science and Engineering, University of Utah, Salt Lake City, Utah 84112

Contents

Abstract

A micromechanics of damage analysis is typically a two-step process. The first step is to use micromechanics to analyze the stresses in a composite in the presence of damage. The second step is to use failure criteria to predict the conditions under which that damage gets larger. This chapter illustrates micromechanics of damage methods with a detailed review of microcracking in cross-ply and related laminates. We review experimental observations, stress analysis methods used to approximate the stresses in the presence of micro-cracks, and the various failure criteria used to predict the development of microcracking damage. We show that the bulk of the stress solutions in the literature can be reduced to a single one-dimensional equation. Unfortunately the one-dimensional analysis is inadequate for describing the experimental observations. We show that two-dimensional methods, based on variational mechanics, work better. The prediction of damage propagation requires use of some failure criterion. We show that strength based failure criteria are inconsistent with experimental observations. Excellent results are obtained, however, when failure is predicted with an accurate energy release rate failure criterion. In addition to microcracking during static loading, some discussion is given about experiments and analysis of microcracking during fatigue, microcracking during thermal cycling, the initiation of delaminations at the tips of microcracks, and the phenomenon of curved microcracking.

1. Introduction

The process by which high-performance composites are damaged and eventually fail is very complex. The complexity is a consequence of material anisotropy and heterogeneity. In homogeneous materials such as metals, polymers, or ceramics, damage can be monitored by observing the growth of a dominant crack. The conditions under which the dominant crack grows and leads to material failure is by definition the field of fracture mechanics [1]. When material properties are homogeneous and isotropic, it is possible to construct a general analysis for the stress distribution near crack tips [2]. This analysis shows that the stress distribution has the same form for all cracks and that in a mathematical sense all cracks in isotropic, homogeneous materials are of the same type. The differences between cracks in isotropic, homogeneous materials, if any, are only due to differences in stress intensity factors. The stress intensity factor is only a function of crack dimension, specimen geometry, and specimen loading conditions.

In contrast, the heterogeneity of composites leads to a variety of damage modes. For example damage can start by matrix cracking, fiber breakage, interfacial debonding between the matrix and the fiber, or delamination between plies. An increase in damage can result from the propagation of the initial damage or from the initiation of a new type of damage. In contrast to isotropic, homogeneous materials that have only one type of crack, composites have many types of cracks. We treat each damage mode as having a unique type of crack. In contrast to cracks in isotropic, homogeneous materials that are typically through-the-thickness cracks that are observable on the surface, many composite cracks are sublaminate cracks that are confined to one or a few plies and may never penetrate to the laminate surface. The concept of stress intensity factor, so useful in isotropic, homogeneous materials, is less significant and often cumbersome in composite materials. Its major advantage is its ability to reduce the description of a crack to a single scalar quantity depending only on crack dimension, specimen geometry, and specimen loading conditions. A similar reduction is not possible for cracks in composites because the crack tip stress field also depends on local environment and crack orientation due to the heterogeneity and anisotropy of composites, respectively.

Before composite laminates can be used with confidence we must extend fracture mechanics to predict under what conditions composite cracks grow and cause laminate failure. Because cracks in composites differ from those in isotropic, homogeneous material, we have, in effect, many new fracture mechanics problems to solve. We also recognize the possibility that one type of crack may influence the initiation and propagation of another type of crack. Part of the work involved in solving the new problems must therefore also include interactions between all possible crack types.

Two popular approaches to composite damage analysis are continuum damage mechanics and microme-chanics of damage. In continuum damage mechanics all damage states are generalized into a damage tensor expressing the state of damage that may include matrix cracking, fiber breakage, interfacial debonding, or ply delamination [3–5]. The composite is then treated as a continuum under states of stress and strain and one seeks to find constitutive relations between stress, strain, and damage. The practical goal is to express

the mechanical properties as functions of damage. If successful, lifetimes of composites can be predicted by determining the level of damage that reduces mechanical properties below some critical values. For further discussion of this approach see Chapters 2 and 3 in this volume. Despite the potential practical importance of continuum damage mechanics, it uses no fracture mechanics or crack propagation theories and therefore does not make any predictions about damage propagation. It only seeks to describe the relation between the mechanical properties and the level of damage. To be useful, continuum damage mechanics requires additional experimental or theoretical input. Experimental input is normally in the form of measured mechanical properties in the presence of a known amount of damage. Theoretical input is normally in the form of predictions of the effect of specific types of damage on macroscopic properties. To provide theoretical input one can no longer consider the composite as a continuum but must specifically consider the effect of damage on local stress states.

The analysis of the various types of damage found in composite materials and the individual predictions of their initiation and growth processes is defined as "micromechanics of damage." This chapter outlines the general procedures used in the micromechanics of damage approach. The complete process is illustrated by a comprehensive review of matrix microcracking and microcrack induced damage in cross-ply and related laminates. A complete micromechanics of damage analysis involves four steps:

(1) Observation of damage

(2) Micromechanics in the presence of damage

(3) Failure criteria and damage propagation prediction

(4) Comparison to experiment

The first step is to determine the type of damage observed in representative composite laminates. This step should be obvious but, surprisingly, is skipped by many investigators. The goal of this step is to understand what type of cracks form, where the cracks form, and what causes them to form. Some typical questions to ask are: Is the damage matrix cracking, fiber breakage, interfacial debonding, or ply delamination? How is the damage process affected by laminate structure and material properties? It is necessary to obtain a large data base of experimental observations before it is possible to develop a meaningful micromechanics of damage analysis.

The second step is the step that distinguishes the micromechanics of damage approach from continuum damage mechanics. Instead of treating the material as a continuum, this step is to undertake a stress analysis in the presence of damage. If the first step was done correctly the stress analysis will be carried out for stress and strain distributions in the presence of observed damage. Unlike isotropic, homogeneous materials for which exact linear elastic solutions are often possible to obtain, analysis of stresses in composite materials almost always requires approximate stress analyses. The key to a successful micromechanics of damage analysis is the development of a mechanics model that leads to a sufficiently accurate stress analysis. For very complex problems involving complex damage states or significant three-dimensional effects, it may be necessary to turn to numerical stress analyses such as finite element analysis. The overuse of numerical analysis, however, tends to limit practical utility, limit model generality without additional costly numerical calculations, and limit physical insights gained from closed form, but approximate stress analyses.

Armed with information about the effect of observed damage on the stresses, the third step is to postulate failure criteria and predict initiation and growth of damage. Failure criteria are usually maximum stress or strain criteria, or fracture mechanics criteria such as stress intensity factor or strain energy release rate. An important feature, often missed in criticism of the literature, is that steps two and three are totally independent. Any available stress analysis can be used with any failure criterion. If experimental results reveal that a particular model for micromechanics of damage is inadequate, it may be the result of the inadequacy of only one step. For example, a good stress analysis coupled with an inappropriate failure criterion will give poor results as will an over simplified stress analysis coupled with a good failure criterion.

Step four is to compare the predictions of steps two and three to the experimental observations in step one. A good micromechanics of damage analysis is defined as one that correlates and explains most or all of the experimental observations.

Four years before his death, renowned chemist Henry Eyring described himself as a "model builder." [6] Three of his four comments about models are relevant to micromechanics of damage analyses:

(1) Models should start out simple and definite enough that predictions are made.

(2) A model is of limited value except as it correlates a substantial body of observable material.

(3) Models that suggest new experiments, even if the theory must be modified, can be useful.

His first comment is about steps two and three. Those two steps should allow predictions to be made about damage processes in composite laminates. To be a general micromechanics of damage analysis it should be possible to make predictions for a wide range of materials and laminate structures. His second comment is about step four. Any micromechanics of damage analysis must be considered incomplete and unsupported unless it is correlated with experimental observations. The true test of any analysis is its ability to be correlated with experimental data from many different laminate structures and materials rather than a few carefully chosen examples. His third comment relates to partially unsuccessful micromechanics of damage analyses. Composite fracture problems are very complex and we have rarely seen a single fracture model that explains all aspects of damage initiation and propagation. Despite the expectation that no model will be perfect, the process of micromechanics of damage is useful if it gives us new insight into composite failure or if it suggests new areas for fruitful study of composite failure.

A Case Study of Matrix Microcracking

The process of micromechanics of damage analysis is best illustrated by examples. The example reviewed in this chapter is the analysis of matrix microcracking and microcrack induced damage in organic-matrix, high-performance composites. Many observations have confirmed that the first form of damage in general angle-ply laminates loaded in tension is matrix cracking or microcracking in the off-axis plies [7–50]. Microcracks are readily observed in 90° plies in which they are logically termed transverse cracks. Even if 90° plies are not present, however, microcracks can still form in the plies with the highest angle with respect to the loading direction (*e.g.* the θ plies in a $[0/\theta/-\theta]_s$ laminate [51]). Microcracks are observed during static loading, fatigue loading, thermal loading, or any combination of these loadings.

The initial effects of a few microcracks in 90° plies are relatively minor. Microcracks cause changes in mechanical properties of the laminate including a reduction in longitudinal stiffness [22] and a change in thermal expansion coefficients [52, 53]. Microcracks introduce pathways through which corrosive agents can penetrate into the interior of the laminate. The mere presence of microcracks and the above minor effects may cause a technical failure [16]. If small changes in mechanical properties can not be tolerated or if leakage is crucial (e.g. for pressure vessels), the presence of the first microcrack causes structural failure. For these critical applications the micromechanics of damage analysis must be able to predict the initiation of microcracking.

More typical composite applications are not affected by a few microcracks and it is tempting to consider microcracking damage to be tolerable as long as the microcrack density is low. Unfortunately there is much evidence suggesting that microcracks act as nuclei for further and potentially more deleterious forms of damage [16]. Microcracks can promote delamination between the off-axis ply (*e.g.* the 90° ply) and the adjacent ply. These delaminations initiate along the line where the edge of the microcrack meets the ply interface. When 0° plies are adjacent to 90° plies, the microcrack can induce longitudinal splitting in the 0° plies. The intersection of the microcrack and the longitudinal split is an area of intense stress concentration that can cause delamination [36, 37]. At late stages of microcracking damage, curved or oblique microcracks may appear near existing straight microcracks [37]. Delamination appears to proceed easily from the tips of curved microcracks [37]. Matrix microcracks in 90° plies and the types of damage induced by matrix microcracks are shown in Fig. 1. A successful micromechanics of damage analysis for matrix microcracking should be capable of predicting not only microcracking, but also the nucleation of other forms of damage.

We list some goals for a successful micromechanics of damage analysis of composite microcracking:

(1) Predict microcrack initiation.

(2) Predict the increase in density of microcracks on continued loading.

(3) Predict the conditions that lead to related forms of damage such as delamination, longitudinal splitting, and curved microcracks.

(4) In the micromechanics analysis, include residual thermal stresses and thereby assess the role of thermal stresses in the damage process.

(5) Predict the effect that microcracks and other forms of damage have on mechanical and thermal properties.

(6) Combine all above results to predict fatigue lifetimes during mechanical fatigue or thermal cycling.
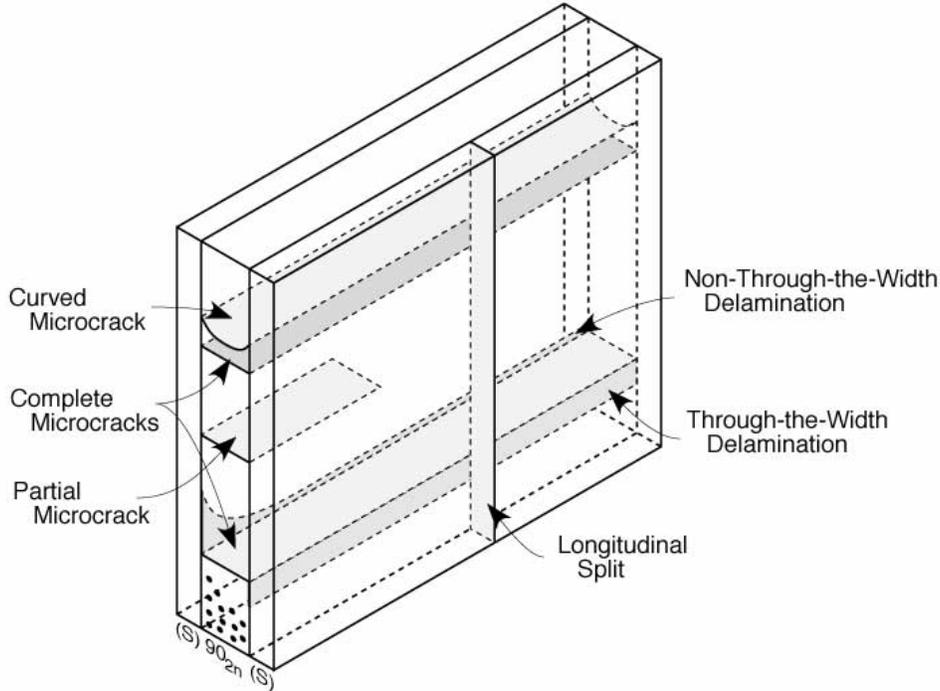
Fig. 1. A $[0_n/90_m]_s$ laminates with several types of damage modes. The illustrated damage modes are complete microcracking, partial microcracking, microcrack induced delamination (both through-the-width delamination and non-through-the-width delamination that initiates at a free edge), curved microcracks, and longitudinal splitting

We review the literature attempts at achieving these goals. With a few exceptions, experimental results and analytical efforts have concentrated on microcracking in 90° plies. To generalize the analysis, we review microcracking in $[(S)/90_n]_s$ and in $[90_n/(S)]_s$ laminates where (S) is any orthotropic sublaminate whose stiffness is relatively larger than the 90° plies. The former laminate has 90° plies clustered around the center of the laminate and the latter has 90° plies on the outer surfaces.

2.   Experimental Observations

The first step in any micromechanics of damage analysis is to observe the damage process Several early investigations show that the first form of failure in high-performance laminates is typically matrix microcracking [7–10]. Since then numerous studies have focused on microcracking and microcrack induced damage in $[(S)/90_n]_s$ and $[90_n/(S)]_s$ laminates [11–50]. In this section we review the experimental observations in those studies.

2.1.   *Microcracking in $[0_m/90_n]_s$ Laminates*

The first systematic study of microcracking in $[0_m/90_n]_s$ laminates that includes the effect of laminate structure is the work of Garrett, Bailey, *et. al.* [11–18]. Their experiments were on glass-reinforced polyester [11, 12] (Tyglas Y119/Crystic 390) and glass-reinforced epoxy [13–17] (E glass/Shell Epikote 828). They varied the thickness of the 90° plies while keeping the thickness of the 0° plies constant at 0.5 mm. As seen in Fig. 2 the strain to initiate microcracking increases as the thickness of the 90° plies decreases [13]. When the 90° plies are thicker than 0.4 mm, the microcracks instantaneously form and span the entire cross-section of the 90° plies. For these thick laminates it is not possible to observe initiation and growth of individual microcracks. For 90° plies between 0.1 mm and 0.4 mm thick, partial microcracks initiate at the free-edges and slowly propagate across the entire width of the laminate. When the 90° plies are less than 0.1 mm thick, no microcracks or partial edge microcracks form before complete laminate failure [13]. These experiments illustrate a microcrack suppression effect as the relative stiffness of the supporting 0° plies increases with
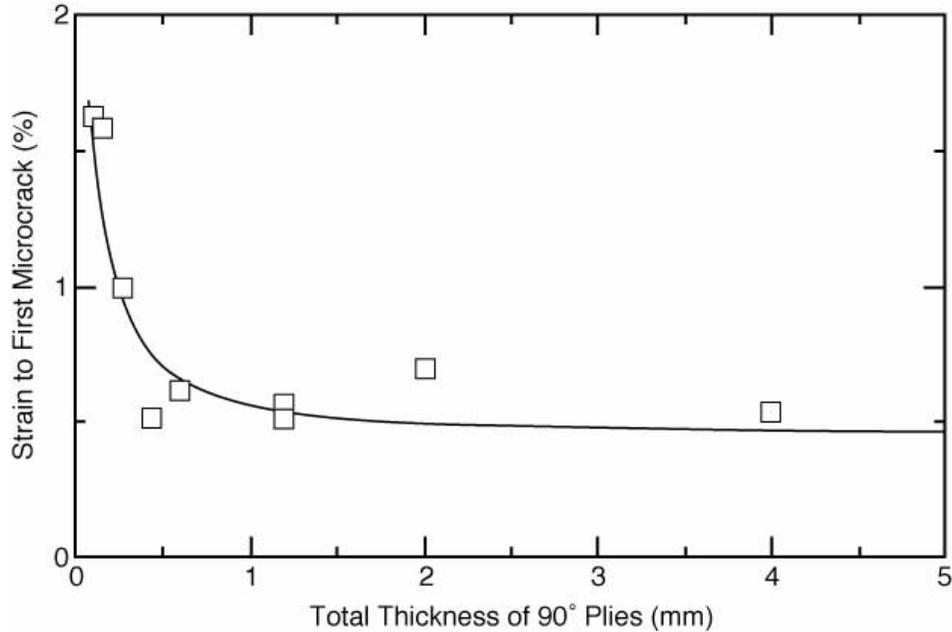
Fig. 2. The strain to initiate microcracking in E glass/Shell Epikote epoxy [0/90/0] laminates as a function of the total thickness of the 90° plies. The 0° plies each have a constant thickness of 0.5 mm. The data in from Ref. [13].

respect to the 90° plies. Upon decreasing the thickness of the 90° plies, the suppression effects begins at the first observation of a partial microcrack. These partial microcracks occur when the 90° plies are 0.4 mm thick or about equal to the thickness of each 0° ply group (0.5 mm). Using stacking sequence nomenclature, the suppression effect begins in these $[0_m/90_n]_s$ laminates when $n \leq \frac{m}{2}$.

Similar microcrack initiation experiments have been done on carbon/epoxy laminates (carbon fiber type II/epoxy [15, 16] and T300/Fiberite 934 epoxy [19]). The results are similar showing an increase in the strain to initiate microcracking as the thickness of the 90° plies decreases. The microcracks in carbon/epoxy laminates generally span the cross section of the 90° plies instantaneously and show less evidence of suppression effects. The reduced microcrack suppression is due to experimental results being confined to laminates with relatively thick 90° plies. According to the results with glass/epoxy laminates, microcrack suppression effects are expected for $[0_m/90]_s$ laminates when $m \geq 2$ and complete suppression is expected only when $m \geq 10$. Most experimental results are confined to $[0_m/90_n]_s$ laminates with $m \leq n$ and thus suppression effects are reduced.

Careful microscopy has been used to investigate the origins of microcrack initiation. At the laminate edge of glass/polyester laminates the microcracks are generally associated with voids and regions of high fiber volume fraction, although microcracks across resin rich areas are sometimes observed [11]. Stress whitening is observed in some glass/epoxy laminates at strains below that required for microcrack initiation [14–17, 20]. Optical microscopy reveals that the stress whitening effect is due to debonding at the interface between the fiber and the matrix. The stress whitening effect is partially reversible by unloading and completely reversible by thermal treatment [14]. To understand stress whitening and microcrack initiation, Bailey and Parvizi [17] studied glass/epoxy laminates with thin 90° plies or laminates in which microcrack formation proceeds by initial edge cracks and slow propagation across the sample width. As strain is increased, the fiber debonds associated with the stress whitening coalesce and eventually form a microcrack. This microcrack propagates from the edge and across the laminate width. Microcracks forming inside the laminate and propagating to the edges are usually not observed. The transparency of glass/epoxy laminates makes these observations possible.

Because carbon/epoxy laminates are opaque, no stress whitening is observed and it is not possible to rule out microcracks forming in the laminate interior. All available evidence, however, suggests that the microcrack formation processes in carbon/epoxy laminates and glass/epoxy laminates are similar. Edge optical microscopy suggests the carbon/epoxy laminate microcracks also initiate at fiber debonds [15]. These

observations are supported by acoustic emission data that associate fiber debonding with microcrack formation [16].

The following description is consistent with experimental observations. At very low strain, stress concentrations at the fiber/matrix interface cause fiber/matrix debonding at specimen free edges. At slightly higher strains these fiber debonds coalesce to form a partial microcrack emanating from the free edge and propagating towards the laminate interior. Eventually the microcrack propagates across the entire cross section of the 90° plies and a complete microcrack forms. This microcrack formation proceeds instantaneously when the the 90° plies are thick and is partially or totally suppressed when the 90° plies are thin.

The initial microcracks usually stop at the 90/0 interface without causing delamination [11, 14]. Continued loading generally leads to the formation of more microcracks. A logical experiment is to count the number of microcracks during loading and plot the microcrack density as a function of applied load. Many investigators have done such experiments on $[0_m/90_n]_s$ laminates. Microcrack density results have been reported for glass/polyester (Tyglas Y119/Crystic 390 [11]), glass/epoxy (E Glass/Shell Epikote 828 [13–15, 17, 20, 21], Scotch Ply 1003 [22], E glass/Ciba Geigy 913 epoxy [23], E glass/epoxy [24]), carbon/epoxy (carbon fiber type II/epoxy [15], T300/Fiberite 934 epoxy [25–29] AS4/Hercules 3501-6 epoxy [25, 26, 29–33], Fibredux 914C [34], Courtaulds XAS/Ciba Geigy 914 epoxy [23, 35], AS4/Hercules 3502 [37]), carbon/toughened epoxy (AS4 Tactix® 556 [30], AS4 Tactix® 695 [30], IM7/8551-1 [30], T300/Fiberite 977-2 [29]), carbon/polycyanate (AS4/Dow polycyanate [30–38], G40-800/rubber modified Dow polycyanate [38]), and carbon/thermoplastic (IM6/duPont Avimid®K Polymer [29], AS4/ICI PEEK [29]. The results for all these laminates are qualitatively similar. Some typical results for two different IM6/duPont Avimid®K Polymer laminates are given in Fig. 3 [29]. After formation of the first microcrack there is a rapid increase in microcrack density with increasing applied load. Eventually the rate of increase in microcrack density slows down and there are signs of reaching a saturation level of damage. Some have termed the final damage state a characteristic damage state [39]. As observed during microcrack initiation experiments, the laminate with thicker 90° plies begins damage at a lower stress level than the laminate with thinner 90° plies. From Fig. 3 it is observed that the saturation microcrack density is lower in laminates with thicker 90° plies. Differences in microcrack density results from one material type to another can be associated with laminate flaws or with material toughness. All laminates have processing flaws. Some of these flaws can initiate microcracks at very low strains resulting in microcracks being observed before the characteristic rapid rise in microcrack density [29]. The absolute load at which microcracks form and the microcrack density rapidly increases is a function of the material toughness. Predictably, laminates with toughened resins usually require higher loads to cause significant levels of microcracking [29, 30]. Similarly, laminates with high strain to failure matrices require higher strains to initiate microcracking [12].

2.2. Delamination in $[0_m/90_n]_s$ Laminates

Although delamination is rarely observed after formation of the first microcrack, it is commonly observed at high microcrack densities [11, 13, 14, 16, 23, 29, 36, 37]. When delamination is observed, it initiates at the 90/0 interface around the tip of an existing microcrack. The delamination process typically occurs just prior to specimen failure [11, 14, 23, 37]. When the 90° plies are very thick, however, delamination is sometimes observed at low microcrack densities and may even occur after the first microcrack [13, 16, 29, 33]. In one of the few systematic studies of delamination in $[0_m/90_n]_s$ laminates, Parvizi and Bailey [14] find that the critical strain for delamination decreases as the 90° ply thickness increases.

The experimental results for delamination are mostly qualitative, but the following description emerges. Microcrack tips at 90/0 interfaces represent regions of high stress concentration that can potentially nucleate delamination. Delamination can occur in almost any laminate but its likelihood increases as the thickness of the 90° plies increases. If the 90° plies are thick enough, it is possible for delamination to initiate from the first microcrack.

2.3. Longitudinal Splitting in $[0_m/90_n]_s$ Laminates

Due to the mismatch of Poisson ratios between 0° and 90° plies, tensile loading of $[0_m/90_n]_s$ laminates leads to a transverse tensile strain in the 0° plies. If this transverse strain gets large enough, the 0° plies can fail by a longitudinal split running parallel to the fibers and the applied load (see Fig. 1) [15, 16,
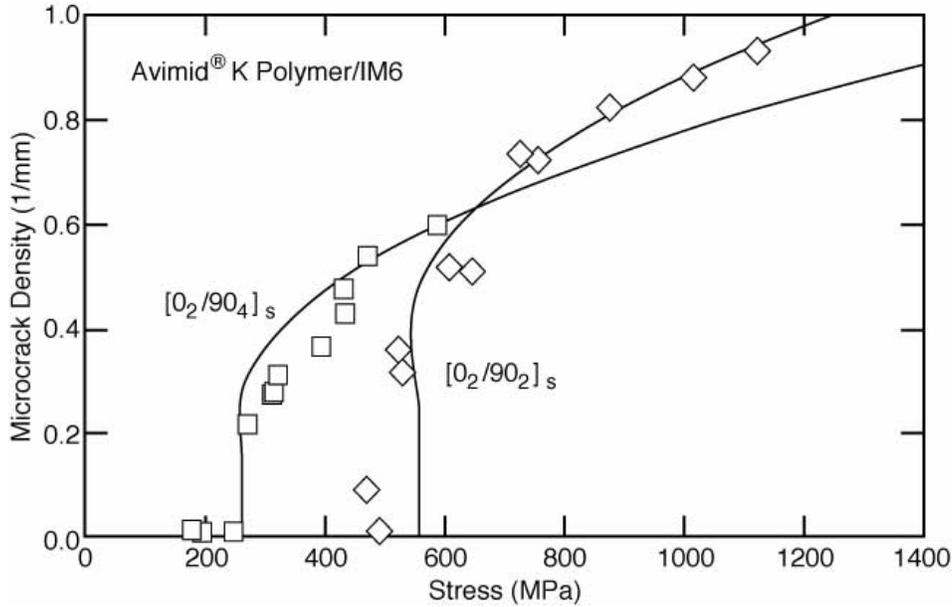
Fig. 3. The microcrack density as a function of applied load in IM6/duPont Avimid$^\circledR$ K Polymer cross-ply laminates. The symbols are experimental data points and the smooth lines are predictions using an energy release rate approach and a variational mechanics stress analysis. Data and predictions are from Ref. [29].

21, 23, 24, 36, 37]. Bailey *et. al.* [15, 16] report seeing longitudinal splitting in glass/epoxy laminates (E glass/Shell Epikote 828) but not in carbon fiber type II/epoxy laminates. Their conclusion is that the strain to failure of the carbon/epoxy laminates is lower than that of glass/epoxy. At the lower strains in the carbon/epoxy, the transverse strain in the $0°$ plies induced by the Poisson ratio mismatch is too low to cause longitudinal splitting. Bader *et. al.* [16] find that the strain to initiate longitudinal splitting increases as the thickness of the $0°$ plies decreases. In analogy with suppression effects in microcracking, the longitudinal splitting propagates across the cross section of the $0°$ plies instantaneously when the $0°$ plies are thick, and propagates slowly when the $0°$ plies are thin [16]. Boniface and Ogin [21] note that longitudinal splitting often initiates at the grips. Although longitudinal splitting is uncommon in carbon/epoxy laminates, it is observed during fatigue (in carbon fiber type II/epoxy [23]) and at late stages of damage (in AS4/Hercules 3502 [37]).

2.4. Microcracking and Delamination in $[(S)/90_n]_s$ Laminates

The microcracking properties of $[\pm\theta/90_n]_s$ laminates are qualitatively similar to those of $[0_2/90_n]_s$ laminates. The reduced stiffness of the $(\pm\theta)$ sublaminate *vs.* the (0_2) sublaminate, however, leads to a loss of constraint, a reduction in the microcrack suppression mechanism, and the formation of microcracks at lower applied loads. Flaggs and Kural [19] observed microcrack initiation in $[\pm\theta/90_n]_s$ carbon/epoxy laminates (T300/Fiberite 934 epoxy) for $\theta = 0°$, $30°$, and $60°$. For all laminates, the strain to initiate microcracking increases as the thickness of the $90°$ plies decreases. The magnitude of the strain increase for thin $90°$ plies (*i.e.* the suppression effect) is reduced for $\theta = 60°$ laminates as compared to $\theta = 0°$ and $\theta = 30°$ laminates. The microcrack density as a function of applied load has been measured for $[\pm25/90_n]_s$ carbon/epoxy laminates (T300/Fiberite 934) [26, 27, 40–42] and for $[\pm\theta/90_n]_s$ carbon/epoxy laminates (AS4/Hercules 3501-6) with $\theta = 0°$, $15°$, and $30°$ [32]. Again the results are very similar to $[0_2/90_n]_s$ laminates. After the formation of the first microcrack there is a rapid rise in microcrack density with increasing load. At higher loads the rate of increase in microcrack density slows and the microcrack densities approach saturation damage states. The major difference is that the reduced stiffness of the $(\pm\theta)$ sublaminate *vs.* the (0_2) sublaminate causes a given level of microcracking damage to occur at a lower level of stress as θ increases.

Interaction between microcracking and delamination is well illustrated by the case study of $[\pm25/90_n]_s$ carbon/epoxy (T300/Fiberite 934) laminates for $n = \frac{1}{2}$, 1, 2, 3, 4, 6, and 8 [26, 27, 40–42]. The choice of

the (± 25) sublaminate was made to promote edge delamination effects. The role of edge delamination in these laminates is therefore greater than it is in typical cross-ply laminates. With the exception of the $n = \frac{1}{2}$ laminate, the initial form of damage is microcracking in the $90°$ ply groups. Laminates with $n \leq 3$ (including $n = \frac{1}{2}$) show thumbnail shaped edge delaminations along the laminate midplane. These edge delaminations are not associated with microcracks, but in the presence of microcracks they sometimes divert to the $-25/90$ interface. Laminates with $n \geq 4$ show delaminations at the $-25/90$ interface emanating from the tips of existing microcracks. The microcrack induced delaminations initiate at the free edge and propagate into the laminate along the edges of microcracks or in the width direction. The number of microcracks observed before the onset of delamination decreases as n increases (for $n \geq 4$). In summary, when n is sufficiently large, microcracks in the $90°$ plies can cause delaminations at the $-25/90$ interface. These microcrack induced delaminations form more easily as the thickness of the $90°$ plies increases.

Microcracking studies of $[(S)/90_n]_s$ laminates are not limited to $[\pm\theta/90_n]_s$ laminates. Caslini *et. al.*, for example, examined all forms of damage in $[\pm45/0/90]_s$ E glass/epoxy laminates which have $(S) = (\pm45/0)$ [24]. They observe $90°$ ply microcracking, $45°$ ply microcracking, edge delamination at the $90/0$ interface, and microcrack induced delaminations at the microcrack tips in the $45°$ plies. The first form of damage is the $90°$ ply microcracking. This microcracking damage approaches saturation before any other forms of damage occur.

2.5.   *Microcracking and Delamination in $[90_n/0_m]_s$ and $[90_n/(S)]_s$ Laminates*

The microcracking and delamination properties of $[90_n/(S)]_s$ laminates or laminates with the $90°$ plies on a free surface differ from those of $[(S)/90_n]_s$ laminates that have only interior $90°$ plies. Although $[90_n/(S)]_s$ laminates have received much less attention than $[(S)/90_n]_s$ laminates, it is important to understand their fracture properties. Under the right stress conditions, any laminate can be viewed as having outer-ply $90°$ plies. For example, when a $[0_m/90_n]_s$ laminate is subjected to longitudinal and transverse in-plane loading or subjected to thermal loading, it should be viewed as a $[90_m/0_n]_s$ laminate for the transverse loading component.

Bailey *et. al.* [15] describe the first microcracking experiments on $[90_m/0_n]_s$ laminates. They measured the strain to initiate microcracking as a function of $90°$ ply thickness for glass/epoxy laminates (E-glass/Shell Epikote 828). As in $[0_m/90_n]_s$ laminates, the strain to initiate microcracking in $[90_n/0_m]_s$ laminates increases as the thickness of $90°$ plies decreases. For all $90°$ ply thicknesses, however, the strain to initiate microcracking in $[90_m/0_n]_s$ laminates is significantly lower than it is in the corresponding $[0_n/90_m]_s$ laminates. Some similar experiments are reported for carbon fiber type II/epoxy laminates, but only at a constant $90°$ ply thickness [15].

A few studies are focused on later stages of microcrack damage resulting from static or fatigue loading of $[90_n/(S)]_s$ laminates. Experiments have been done on carbon/epoxy (T300/5208 [43], AS4/Hercules 3501-6 [31–33]) and on glass/epoxy (Scotch Ply 1003 [22]); the observations are qualitatively similar to those for $[(S)/90_n]_s$ laminates. Soon after the first microcrack, the microcrack density increases rapidly. At higher loads the rate of increase in microcrack density slows down and tends towards a saturation limit. A significant observation is that the saturation microcrack density is lower in $[90_n/(S)]_s$ laminates than it is in the corresponding $[(S)/90_n]_s$ laminates [32, 43].

The characteristic damage state of microcracking in $[90_n/(S)]_s$ laminates has one interesting difference from that of $[(S)/90_n]_s$ laminates. In $[(S)/90_n]_s$ laminates there is only one $90°$ ply group. At high microcrack density, the $90°$ ply group cracks into an array of roughly periodic microcracks (see Fig. 4A). In contrast, $[90_n/(S)]_s$ laminates have two $90°$ ply groups. At high microcrack density, each $90°$ ply group cracks into an individual array of roughly periodic microcracks. The microcrack density for such a laminate is taken as the average of the microcrack densities in the two $90°$ ply groups. To define the characteristic damage state, it is important to specify the spatial relation between the microcrack patterns in the two $90°$ ply groups. The microcracks in the two $90°$ ply groups are staggered or antisymmetric [22, 31, 32]. That is, the microcracks in one $90°$ ply group are shifted by one-half of a microcrack interval from those in the other $90°$ ply group (see Fig. 4B). Stinchcomb *et. al.* [43] give the sole report of symmetric damage in which the microcracks in one $90°$ ply group are directly opposite the microcracks in the other $90°$ ply groups. The irreproducibility of this result and its inconsistency with new theoretical predictions [31, 54] indicate that the drawing in Ref. [43] might not be based on a careful observation of specimen damage.
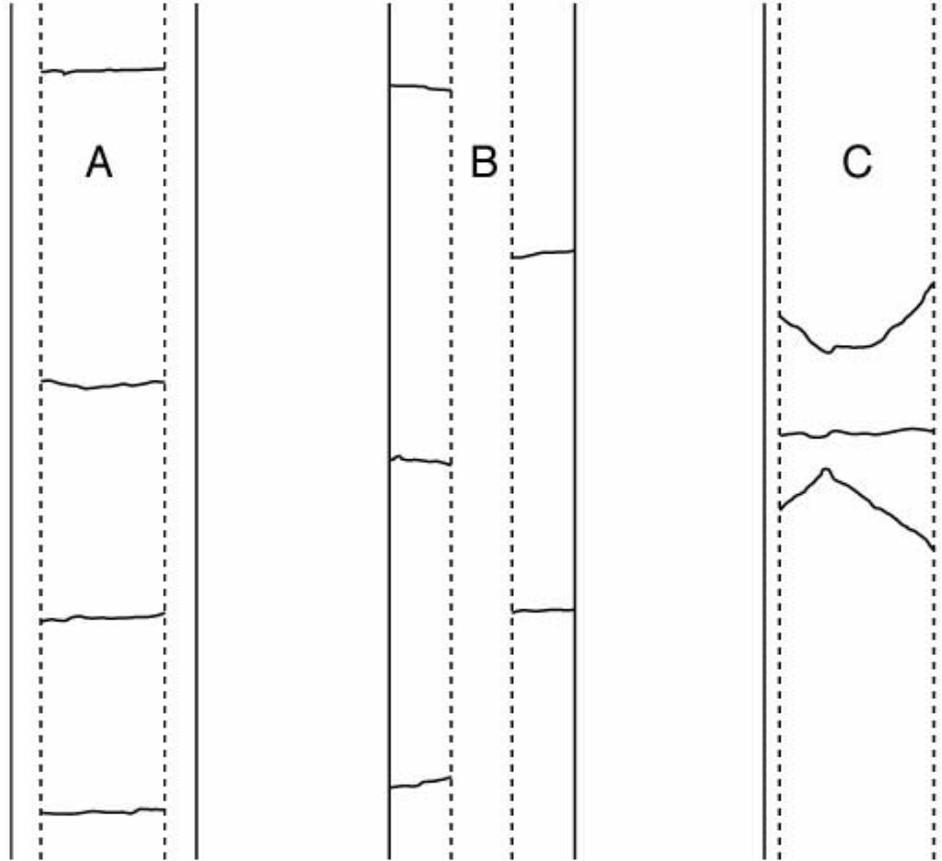
Fig. 4. Sketches of actual edge views of typically damaged cross-ply laminates. A. Roughly periodic array of microcracks in a $[0/90_4]_s$ laminate. B. Antisymmetric or staggered microcracks in a $[90_4/0_2]_s$ laminate. C. Two curved or oblique microcracks near one straight microcrack in a $[0/90_8]_s$ laminate.

The antisymmetric damage state influences the delamination process in $[90_n/(S)]_s$ laminates. As described later, the antisymmetric damage state induces a local bending moment at existing microcracks that increases the mode I or opening mode component of the delamination process [54]. The result of increased loading for mode I fracture is that delamination initiates more easily in $[90_n/(S)]_s$ laminates than it does in the corresponding $[(S)/90_n]_s$ laminate. Three experimental observations confirm this effect. Caslini *et. al.* [24] did microcracking experiments on $[\pm45/0/90]_s$ E glass/epoxy laminates. At late stages of damage, microcracks develop in the $+45°$ and the $-45°$ plies. Microcrack induced delaminations are more commonly associated with the outer-ply microcracks than with microcracks in the inner $90°$ plies [24]. Nairn and Bark [32] and Jen and Sun [33] studied microcracking in $[(S)/90_n]_s$ and $[90_n/(S)]_s$ carbon/epoxy laminates (AS4/Hercules 3501-6) and find the $[90_n/(S)]_s$ laminates more prone to microcrack induced delaminations. Adams *et. al.* [47] studied thermally induced microcracking. Delamination is common in $[90_3/0]_s$ laminates or laminates with thick outer-ply $90°$ plies [47].

2.6. Curved or Oblique Microcracks

At low microcrack densities, new microcracks in $[(S)/90_n]_s$ laminates tend to form approximately midway between existing microcracks. At high microcrack densities, curved or oblique microcracks are observed to initiate at the $90/(S)$ interface [11, 14, 23, 37, 35]. The curved microcracks make an angle of 40-60° with respect to the interface [11, 14, 23, 37, 35] and are always associated with existing straight microcracks [37] (see Fig. 4C). The typical curved microcrack forms about one ply thickness away from an existing straight microcrack [35, 37]. As the thickness of the $90°$ plies increases, the strain to initiate curved microcracks decreases [14] and more curved microcracks form before the laminate fails [37].

2.7. Mechanical Fatigue Experiments

Microcracking fatigue experiments have been done on carbon/epoxy (T300/5208 [43], T300/Fiberite 934 [44], Courtaulds XAS/Ciba Geigy 914 epoxy [23]), glass/epoxy (Scotch Ply 1003 [22], E-glass/epoxy [45, 46, 24]), carbon/thermoplastic (IM6/duPont Avimid® K Polymer [44]), and carbon/polycyanate (AS4/Dow polycyanate [38], G40-800/rubber modified Dow polycyanate [38]). The typical experiments are to measure microcrack density and stiffness reduction as functions of cycle number.

Early fatigue results suggested that laminates prone to microcracking damage form a characteristic damage state that is a function of the stacking sequence but perhaps independent of the loading process [22, 43]. Although qualitatively correct, observations of differences in the type and amount of damage resulting from static loading *vs.* fatigue loading show that the characteristic damage state is an oversimplification [21, 23, 24, 35]. In general, more secondary damage modes such as longitudinal splitting, delamination, and curved microcracks are observed in fatigued specimens than in specimens loaded in static tension [23, 24].

The mechanism of microcrack propagation is also different during fatigue. In static loading, microcrack propagation is governed by the thickness of the $90°$ plies. When the $90°$ plies are thick, the microcrack propagation is instantaneous; when the $90°$ plies are thin, the microcrack propagation is controlled or perhaps even suppressed. During fatigue loading, microcrack propagation still depends on the thickness of the $90°$ plies but also depends on the magnitude of the maximum applied stress — σ_{max} [21, 35]. When σ_{max} is below the static stress to initiate microcracks, new microcracks initiate at the specimen edge and propagate slowly across the specimen width. When σ_{max} is above this static stress, the microcracks that initiate at low microcrack density span the $90°$ ply width instantaneously while the microcracks that initiate at high microcrack density propagate slowly across the specimen width [21, 35]. Although most microcracks form at specimen edges, some are observed to form in the middle of the laminate [21].

2.8. Thermally Induced Microcracks

The mismatch of the thermal expansion coefficients between the (S) sublaminate and the $90°$ plies means that the individual plies will be under residual stress or thermal load. As an $[(S)/90_n]_s$ laminate is cooled, an x-direction tensile stress develops in the $90°$ plies balanced by an x-direction compressive stress in the (S) sublaminates. If the tensile stress gets high enough, the $90°$ plies can microcrack. In some laminates a single cooling to sub-zero temperatures can initiate microcracks [47–50]. Thermal cycling, between -250°F and +250°F (-156°C and 121°C) for example, causes the microcrack density to increase with cycle number [47, 50]. Most features about microcracking that are observed for mechanical loading are also observed for microcracks caused by thermal loading. In particular, microcracks initiate at the free edge and usually propagate instantaneously across the sample width, thicker $90°$ ply groups microcrack more easily, and microcracks can induce delamination at the $90/(S)$ interface [47].

A unique feature of thermally induced microcracking in $[0_m/90_n]_s$ laminates is that thermal loading is biaxial. When viewed along the standard edge — the edge parallel to the $0°$ plies — the laminate is seen as a $[0_m/90_n]_s$ laminate. In this direction the thermal stress in the central $90°$ plies is tensile and thermal loading causes microcracking of those plies. If the sample is rotated $90°$, the laminate is seen as a $[90_n/0_m]_s$ laminate. In this direction the thermal stress in the outer $90°$ plies is tensile and thermal loading causes outer-ply microcracking. When viewed from both directions, thermal loading of $[0_m/90_n]_s$ laminates causes microcracking in all plies [47, 50]. The number of microcracks developed in the $0°$ or $90°$ plies depends on the thicknesses of those ply groups and on the dimensions of the plate.

3. Stress Analysis

An important step of any micromechanics of damage analysis is to obtain the stress states for damaged laminates. We begin with laminates damaged only by microcracks in the $90°$ plies. Other damage modes, such as delamination and curved microcracks, are considered later. The laminate coordinate system is defined in Fig. 5. The x direction is the loading direction; the y direction is the width direction; the z direction is the thickness direction. The sample length (L), width (W), and thickness (B) are also shown in Fig. 5.

We simplify the microcrack damage state by assuming that all microcracks instantaneously span the entire cross-section of the $90°$ plies. This assumption is reasonable because partial microcracks are only
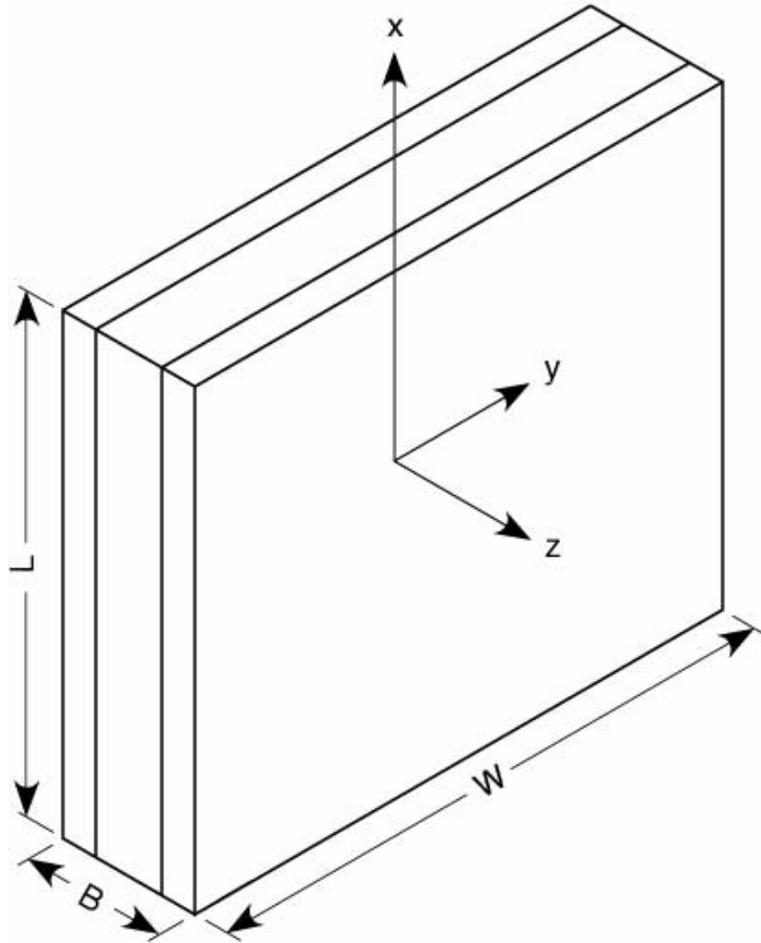
Fig. 5. The coordinate system for the stress analysis of $[(S)/90_n]_s$ and $[90_n/(S)]_s$ laminates. L, W, and B are the length, width, and thickness of the laminate plate.

observed in unusual circumstances such as laminates with thin $90°$ plies [13] or laminates under low-stress fatigue [21, 35]. A microcrack that spans the entire cross-section of the $90°$ plies is a through-the-width microcrack. In the presence of only through-the-width damage, the stress analysis is approximately two-dimensional in the $x - z$ plane. The coordinate system for the $x - z$ stress analysis of $[(S)/90_n]_s$ laminates is given in Fig. 6A. The "unit cell" of damage is the area between two existing microcracks. We define t_1 as the semi-thickness of the $90°$ ply group, t_2 as the thickness of each (S) sublaminate, and $2a$ as the distance between existing microcracks.

In the analysis of $[90_n/(S)]_s$ laminates we must account for the observed staggered microcracks in the two $90°$ ply groups. We idealize the damage state by assuming that microcrack stagger is perfect and take the "unit cell" of damage as the area between two existing microcracks in one of the $90°$ ply groups. The coordinate system for the "unit cell" of damage for $[90_n/(S)]_s$ laminates is given in Fig. 7A. For these laminates t_1 is the total thickness of each $90°$ ply group, t_2 is the thickness of the (S) sublaminate, and $2a$ is the distance between existing microcracks in one of the $90°$ ply groups.

By a few reasonable assumptions, the stress analysis simplifies mathematically to a two-dimensional analysis. The third dimension enters by an additional assumption of plane stress, plane strain, or generalized plane strain conditions. We describe mostly plane stress analyses but realize that a plane strain solution can trivially be generated from a plane stress solution by substituting reduced mechanical properties for the mechanical properties of the plane stress analysis. Although a two-dimensional analysis gives us much information about microcracking damage, it can never yield information about three-dimensional effects. A two dimensional analysis is therefore not useful in predicting the y direction propagation of partial microcracks
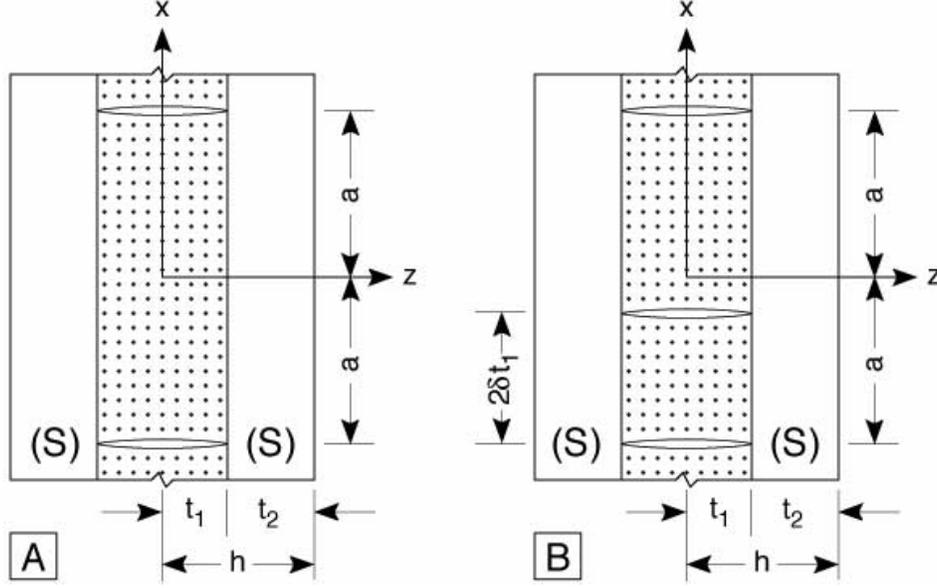
Fig. 6. Edge view of a $[(S)/90_n]_s$ laminate with microcracks. A: Two microcracks in the 90° plies. B: The formation of a new microcrack at a distance $2\delta t_1$ above the bottom microcrack.

or in elucidating the edge effects that cause microcracks to initiate at specimen free-edges.

3.1. Statement of the Problem

We define a component of the stress tensor by $\sigma_{jk}^{(i)}$ where j and k are x, y, or z and superscript (i) denotes the ply group ($i = 1$ for the 90° ply group and $i = 2$ for the (S) sublaminate). In the $x - z$ plane of an undamaged laminate, only $\sigma_{xx}^{(i)}$ is non-zero. Defining $\sigma_{x0}^{(i)}$ as the initial x-axis stress in ply group i, the stresses in the undamaged laminate are

$$\sigma_{xx}^{(i)} = \sigma_{x0}^{(i)} \qquad\qquad \sigma_{zz}^{(i)} = \sigma_{xz}^{(i)} = 0 \tag{1}$$

Because microcracking occurs at very low strains, a linear thermoelastic analysis is appropriate. Linearity allows us to rewrite the initial stresses as

$$sxoi = k_m^{(i)}\sigma_0 + k_{th}^{(i)}T \tag{2}$$

where σ_0 is the total applied stress in the x direction and $T = T_s - T_0$ is the difference between the specimen temperature, T_s, and the stress free temperature, T_0. $k_m^{(i)}$ and $k_{th}^{(i)}$ are mechanical load and thermal stress constants for ply group i.

There are some minor differences in the various microcracking analyses regarding the evaluation of $k_m^{(i)}$ and $k_{th}^{(i)}$. If the third dimension (the y dimension) is ignored, the stress state of an undamaged laminate reduces to a one-dimensional problem. Assuming that the x-direction displacements of all ply groups are identical, one quickly derives

$$k_m^{(1)} = \frac{E_x^{(1)}}{E_c^0}, \quad k_{th}^{(1)} = -\frac{\Delta\alpha}{C_1}, \quad k_m^{(2)} = \frac{E_x^{(2)}}{E_c^0}, \quad \text{and} k_{th}^{(2)} = \frac{\Delta\alpha}{\lambda C_1} \tag{3}$$

where $E_x^{(i)}$ is the x-direction Young's modulus of ply group i,

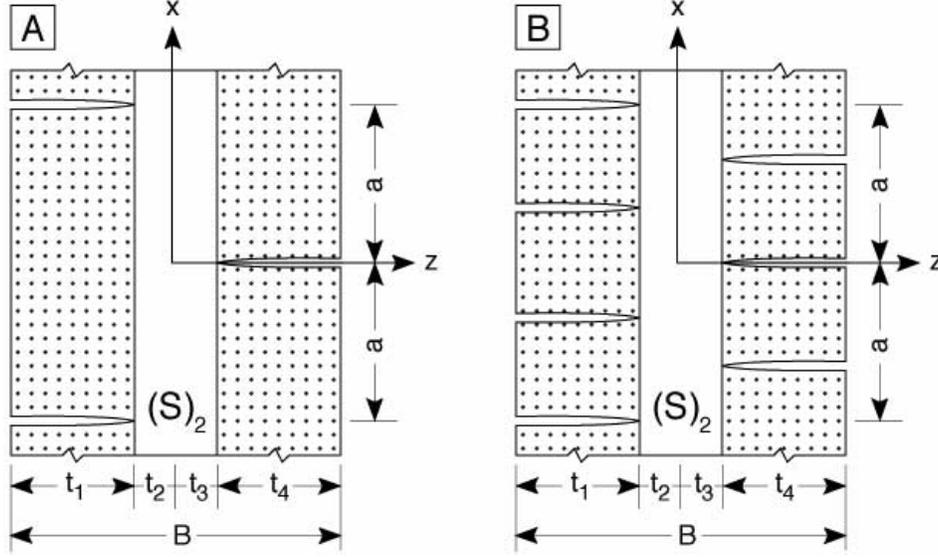$$Ec = \frac{t_1 E_x^{(1)} + t_2 E_x^{(2)}}{t_1 + t_2} \tag{4}$$

Fig. 7. A unit cell of damage in a $[90_n/(S)]_s$ laminate having "staggered" or antisymmetric microcracks. A: A single unit cell of damage. B: Three unit cells of damage after formation of new microcracks at locations of local maxima in tensile stress.

is the rule-of-mixtures x-direction modulus of the undamaged laminate, $\Delta\alpha = \alpha_x^{(1)} - \alpha_x^{(2)}$ is the difference between the x-direction thermal expansion coefficients of the two ply groups,

$$C_1 = \frac{1}{E_x^{(1)}} + \frac{1}{\lambda E_x^{(2)}} \tag{5}$$

and $\lambda = \frac{t_2}{t_1}$.

Alternatively, one may analyze the undamaged laminate using laminated plate theory. Some simple laminated plate theory calculations lead to

$$k_m^{(1)} = \frac{Q_{xx}^{(1)}}{E_{cl}^0}\left(1 - \frac{A_{xy}Q_{xy}^{(1)}}{A_{yy}Q_{xx}^{(1)}}\right) \tag{6}$$

$$k_{th}^{(1)} = -\frac{\left(t_1 t_2 Q_{xx}^{(2)}Q_{yy}^{(1)}E_x^{(1)} + t_2^2 Q_{xx}^{(1)}Q_{yy}^{(2)}E_x^{(2)}\right)\Delta\alpha + \left(t_1 t_2 Q_{xx}^{(1)}Q_{xy}^{(2)}E_y^{(1)} + t_2^2 Q_{xx}^{(2)}Q_{xy}^{(1)}E_y^{(2)}\right)\left(\alpha_y^{(1)} - \alpha_y^{(2)}\right)}{A_{xx}A_{yy} - A_{xy}^2} \tag{7}$$

$$k_m^{(2)} = \frac{Q_{xx}^{(2)}}{E_{cl}^0}\left(1 - \frac{A_{xy}Q_{xy}^{(2)}}{A_{yy}Q_{xx}^{(2)}}\right) \tag{8}$$

$$k_{th}^{(2)} = \frac{\left(t_1^2 Q_{xx}^{(2)}Q_{yy}^{(1)}E_x^{(1)} + t_1 t_2 Q_{xx}^{(1)}Q_{yy}^{(2)}E_x^{(2)}\right)\Delta\alpha + \left(t_1^2 Q_{xx}^{(1)}Q_{xy}^{(2)}E_y^{(1)} + t_1 t_2 Q_{xx}^{(2)}Q_{xy}^{(1)}E_y^{(2)}\right)\left(\alpha_y^{(1)} - \alpha_y^{(2)}\right)}{A_{xx}A_{yy} - A_{xy}^2} \tag{9}$$

where $Q_{jk}^{(i)}$ are elements of the stiffness matrix of orthotropic ply group i in the laminate coordinate system, A_{jk} are elements of the laminate stiffness matrix defined by

$$A_{jk} = t_1 Q_{jk}^{(1)} + t_2 Q_{jk}^{(2)} \tag{10}$$

and E_{cl}^0 is the laminated plate theory result for the x-direction laminate modulus:

$$E_{cl}^0 = \frac{A_{xx}A_{yy} - A_{xy}^2}{(t_1 + t_2)A_{yy}} \tag{11}$$

The mechanical load and thermal stress constants obtained either by simple one-dimensional analysis or by laminated plate theory are identical if the Poisson ratios, $\nu_{xy}^{(i)}$, are set equal to zero. Physically, for laminates under unidirectional tension, laminated plate theory is a correction of the one-dimensional analysis to account for transverse Poisson's contraction. In cross-ply laminates, the correction for Poisson's contraction is generally small. For a homologous series of $[0/90_n]_s$ laminates with $n = \frac{1}{2}$ to 8, the Poisson correction to $k_m^{(i)}$ is always less than 2% and the Poisson correction to $k_{th}^{(i)}$ is always less than 6.5%. Because these correction factors are small, in discussing the literature, we regard consideration of Poisson's contraction as an insignificant aspect. In other words, if the only feature distinguishing two analyses is the inclusion of Poisson's contraction we regard those analyses as identical.

When microcracks form in an undamaged laminate, the stresses change. In general all stress components, $\sigma_{xx}^{(i)}$, $\sigma_{xz}^{(i)}$, and $\sigma_{zz}^{(i)}$, become non-zero. In terms of boundary conditions, it is normally assumed that microcrack surfaces are stress free. Thus the normal and shear stresses in the 90° plies are zero on the microcrack surfaces. The load no longer carried by the 90° plies is transferred to adjacent unbroken plies. For $[(S)/90_n]_s$ laminates these requirements and symmetry in shear stresses lead to the following boundary conditions

$$\left\langle \sigma_{xx}^{(2)}(\pm a) \right\rangle = \sigma_{x0}^{(2)} + \frac{\sigma_{x0}^{(1)}}{\lambda} \tag{12}$$

$$\sigma_{xx}^{(1)}(\pm a) = 0 \tag{13}$$

$$\sigma_{xz}^{(1)}(\pm a) = \sigma_{xz}^{(2)}(\pm a) = 0 \tag{14}$$

where $\left\langle \sigma_{xx}^{(2)}(\pm a) \right\rangle$ is the average x-direction stress in the (S) sublaminate. In the next section we discuss some approximate stress analyses that are incapable of satisfying the zero shear stress boundary conditions in Eq. (14). Such analyses are clearly deficient. The situation in $[90_n/(S)]_s$ laminates is more complex. Because of staggered microcracks, the load lost by microcracking of one 90° ply group is carried by both the $(S)_2$ sublaminate and the other 90° ply group. The analysis of $[90_n/(S)]_s$ laminates is considered in more detail later.

The goal of the stress analysis is to solve for the stress distribution in laminates after the formation of microcracking damage. The boundary conditions for $[(S)/90_n]_s$ laminates are in Eqs. (12)–(14). The next few sections discuss the approximate stress analyses that have appeared in the literature.

3.2.   One-Dimensional Analysis of $[(S)/90_n]_s$ Laminates

Many analyses eliminate the z-dependence of the problem by making various assumptions about the z-direction stress or displacement. The common assumptions are zero stress, zero average stress, or zero displacement. We define any analysis using one of these assumptions as a one-dimensional analysis. Examples can be found in Refs. [11, 15, 20, 39, 45, 46, 56–64]. In this section we show that all one-dimensional analyses can be reduced to a single governing equation. Thus despite much effort in the late 1970's and early 1980's, none of the work in Refs. [15, 20, 39, 45, 46, 56–64] improves on the original 1977 work of Garrett and Bailey [11]. We note that some authors describe their analyses as "two-dimensional" analyses [56, 57, 61, 62]. In all cases, however, the second dimension is the y-dimension whose inclusion is little more than a correction for Poisson's contraction. As discussed in the previous section, the difference between a two-dimensional $x - y$ plane analysis and a one dimensional x-axis analysis is marginal.

We define $\Delta\sigma(x)$ as the total amount of stress transferred from the 90° plies to the (S) sublaminate:

$$\Delta\sigma(x) = \left\langle \sigma_{xx}^{(2)}(x) \right\rangle - \sigma_{x0}^{(2)} \tag{15}$$

Garrett and Bailey [11] use a shear-lag approximation that the rate of stress transfer from the 90° plies to the (S) sublaminate is proportional to the difference of the longitudinal displacements in those two ply groups. They derive a second order differential equation for $\Delta\sigma$. We transpose their equation to a dimensionless x-direction coordinate defined as $\xi = \frac{x}{t_1}$ to get

$$\frac{d^2\Delta\sigma}{d\xi^2} + \phi^2\Delta\sigma = 0 \tag{16}$$

where ϕ^2 is a constant that depends on laminate structure and material properties. By using a consistent nomenclature, we find that all one-dimensional analyses (including the "two-dimensional" $x - y$ plane analyses [56, 57, 61, 62]) can be reduced to a generalized form of Garrett and Bailey's [11] equation:

$$\frac{d^2\Delta\sigma}{d\xi^2} + \phi^2\Delta\sigma = \omega(P) \tag{17}$$

where $\omega(P)$ is a function that may depend on laminate structure, microcrack spacing, and applied load (P). The boundary conditions for the general equation are

$$\Delta\sigma(\pm\rho) = \frac{\sigma_{x0}^{(1)}}{\lambda} \tag{18}$$

where $\rho = \frac{a}{t_1}$ is the dimensionless half-spacing of the microcrack interval. The constant ϕ governs the rate of stress transfer through shear at the $90/(S)$ interface and we call it the shear stress transfer coefficient. The function ω is zero in all analyses except that of Nuismer and Tan [61, 62]. We retain a non-zero ω to group all one-dimensional analyses into a single equation. The fact that the analyses in Refs. [11, 15, 20, 39, 45, 46, 56–64] can all be reduced to the same governing equation, with different ϕ^2 and ω, is evidence that despite some author's claims, all those analyses are mathematically one-dimensional analyses.

Equation (17) is easily solved to give

$$\Delta\sigma = -\frac{\omega}{\phi^2} + \left(\frac{\sigma_{x0}^{(1)}}{\lambda} + \frac{\omega}{\phi^2}\right)\frac{\cosh\phi\xi}{\cosh\phi\rho} \tag{19}$$

The average stress in the (S) sublaminate is

$$\left\langle\sigma_{xx}^{(2)}\right\rangle = \sigma_{x0}^{(2)} - \frac{\omega}{\phi^2} + \left(\frac{\sigma_{x0}^{(1)}}{\lambda} + \frac{\omega}{\phi^2}\right)\frac{\cosh\phi\xi}{\cosh\phi\rho} \tag{20}$$

By force balance, the average stress in the 90° plies is

$$\left\langle\sigma_{xx}^{(1)}\right\rangle = \left(\sigma_{x0}^{(1)} + \frac{\lambda\omega}{\phi^2}\right)\left(1 - \frac{\cosh\phi\xi}{\cosh\phi\rho}\right) \tag{21}$$

Integrating the equations of equilibrium, the load transfer from the 90° plies to the (S) sublaminate by shear at the interface is described by

$$\frac{d\Delta\sigma}{d\xi} = \frac{\tau_i}{\lambda} \tag{22}$$

where τ_i is the interfacial shear stress [11]. With the aid Eqs. (19) and (22), the one-dimensional analyses give the interfacial shear stress as

$$\tau_i = \phi\left(\sigma_{x0}^{(1)} + \frac{\lambda\omega}{\phi^2}\right)\frac{\sinh\phi\xi}{\cosh\phi\rho} \tag{23}$$

The average x-direction tensile stress in the 90° plies and the interfacial shear stress derived from the one-dimensional analysis are plotted in Fig. 8. The plots are for a $[0/90_2]_s$ carbon/epoxy laminate. As required by boundary conditions, $\sigma_{xx}^{(1)}$ is zero on the microcrack surfaces. Away from the microcrack, $\sigma_{xx}^{(1)}$ increases as stress is transferred from the (S) sublaminate back into the 90° plies. The shear stress has a maximum at the microcrack surfaces and decays towards zero. The non-zero shear stress on the microcrack surfaces is a violation of boundary conditions and a deficiency of all one-dimensional analyses.

Having solved the general one dimensional analysis equation (Eq. (17)), the only thing that distinguishes the numerous one-dimensional theories is the procedure used to evaluate ϕ and ω. Garrett and Bailey et. al. [11, 15] describe the first one-dimensional analysis. They use shear-lag approximations and assume that the displacement in the 90° plies is a function of x but is independent of z. They find

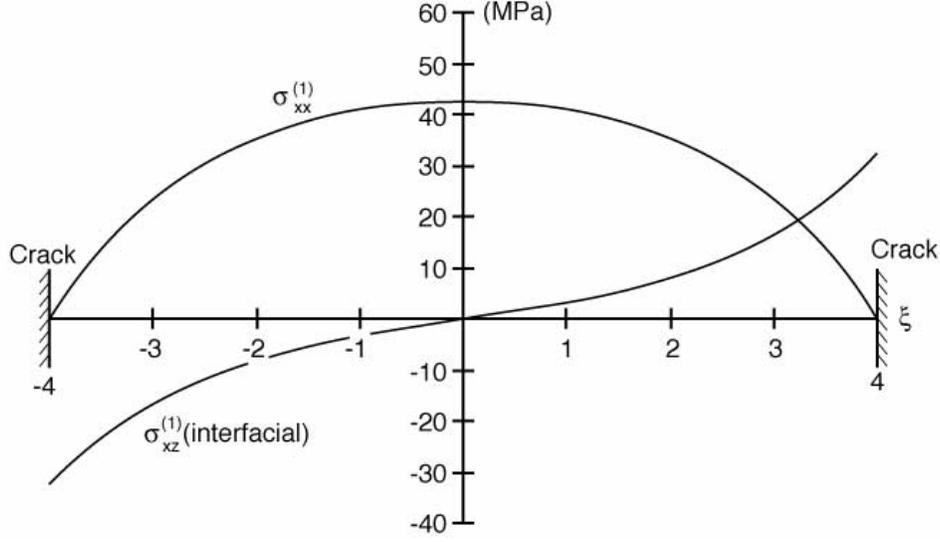$$\phi^2 = G_{xz}^{(1)}C_1 \qquad \text{and} \qquad \omega = 0 \tag{24}$$

Fig. 8. Stresses between two microcracks in a $[0/90_2]_s$ carbon/epoxy laminate from a one-dimensional analysis. The applied stress is 100 MPa, thermal load is $T = -125°C$, and the microcrack spacing is $\rho = 4$. The normal stress $(\sigma_{xx}^{(1)})$ is the average tensile stress in the 90° ply group. The plotted shear stress $(\sigma_{xz}^{(1)})$ is the shear stress at the 90/0 interface.

where $G_{xz}^{(1)}$ is the shear modulus of the 90° plies in the $x - z$ plane and C_1 is defined in Eq. (5). We show later that this first calculation of ϕ^2 is nearly optimal for calculating the effect of microcracks on longitudinal laminate modulus. We note that Garrett and Bailey [11] only solved for stresses around an isolated microcrack. For an isolated microcrack solution, we simply place the microcrack at the origin and solve Eq. (17) with new boundary conditions

$$\Delta\sigma(0) = \frac{\sigma_{x0}^{(1)}}{\lambda} \qquad \text{and} \qquad \Delta\sigma(\infty) = 0 \tag{25}$$

Manders *et. al.* [20] repeat Garrett and Bailey's analysis [11] with the same value of ϕ^2 and ω but extend it to account for neighboring microcracks.

Ogin *et. al.* [45, 46, 64] attempted to improve on the analysis of Garrett and Bailey [11] by making a more realistic assumption that the displacement in the 90° plies is parabolic in z. Unfortunately, the more complicated analysis results in only a trivial change — the value of ϕ^2 is increased by a factor of three. Ogin *et. al.* [45, 46, 64] thus find

$$\phi^2 = 3G_{xz}^{(1)}C_1 \qquad \text{and} \qquad \omega = 0 \tag{26}$$

Han, Hahn, and Croman [58, 59] make the same parabolic displacement assumption and derive results identical to those previously derived by Ogin *et. al.* [45, 46, 64].

Several investigators tried to avoid specifying ϕ by treating it as an adjustable parameter [39, 57, 60]. Physically, the approach is to introduce a shear stress transfer layer between ply groups and assume that this layer carries only shear stress while the plies carry only tensile stress. The effective shear stiffness of the shear stress transfer layer enters ϕ^2 as an adjustable parameter. Reifsnider [39] presents the first use of a shear stress transfer layer. For the specific case of $[(S)/90_n]_s$ laminates, his analysis yields

$$\phi^2 = \frac{Gt_1C_1}{t_0} \qquad \text{and} \qquad \omega = 0 \tag{27}$$

where G is the shear modulus of the shear stress transfer layer and t_0 is its thickness. Fukanaga *et. al.* [57] and Laws and Dvorak [60] adopt the same strategy as Reifsnider [39] and derive identical results for ϕ^2 and ω. A major disadvantage of this approach is that $\frac{G}{t_0}$ or the shear stiffness of the shear stress transfer layer is an unknown parameter that must be determined by fitting experimental results.

Flaggs [56] introduces a "two-dimensional" shear-lag analysis that accounts for both applied normal and shear loadings. The second dimension is the y dimension while the z dimension is eliminated by assuming zero z displacement. His analysis reduces to a system of two coupled second order differential equations. When there is no shear loading, the only remaining equation is identical to the general one-dimensional analysis equation (see Eq. (17)) with

$$\phi^2 = \frac{2\left(\dfrac{1}{\lambda Q_{xx}^{(2)}} + \dfrac{Q_{yy}^{(1)} - \dfrac{Q_{xy}^{(1)}Q_{xy}^{(2)}}{Q_{xx}^{(2)}}}{Q_{xx}^{(1)}Q_{yy}^{(1)} - Q_{xy}^{(1)}{}^2}\right)}{\left(\dfrac{1}{\kappa^2} - \dfrac{1}{2}\right)\dfrac{1}{G_{xz}^{(1)}} + \dfrac{\lambda}{2G_{xz}^{(2)}}} \qquad \text{and} \qquad \omega = 0 \tag{28}$$

where κ is a transverse shear correction factor. Mathematically, Flaggs [56] analysis is a one-dimensional analysis with a minor correction for Poisson's contraction introduced by approximate inclusion of the y dimension. In fact, if we set $\nu_{xy}^{(i)} = 0$ and $\kappa = 1$, ϕ^2 reduces to

$$\phi^2 = \frac{4C_1}{3C_4} \tag{29}$$

where

$$C_4 = \frac{1}{3G_{xz}^{(1)}} + \frac{\lambda}{3G_{xz}^{(2)}} \tag{30}$$

This value of ϕ^2 is similar to the results of Garrett and Bailey $et.$ $al.$ [11, 15] and of Ogin $et.$ $al.$ [45, 46, 64] except that $G_{xz}^{(1)}$ is replaced by $\frac{1}{C_4}$ and the numerical prefactor $\left(\frac{4}{3}\right)$ is between the prefactors of Garrett and Bailey $et.$ $al.$ [11, 15] (1) and Ogin $et.$ $al.$ [45, 46, 64] (3).

Another $x - y$ plane, "two-dimensional" elasticity analysis is described by Nuismer and Tan [61]. Their analysis eliminates the z dimension by setting the average z-direction tensile stress to zero. Although no corresponding equation appears in their paper, their analysis reduces to the general one-dimensional equation by setting

$$\phi^2 = \frac{C_1^*}{C_4} \qquad \text{and} \qquad \omega = \frac{t_1 \tau_i'(a) - \phi^2 \sigma_{x0}^{(1)}}{\lambda} \tag{31}$$

where C_1^* is the same as C_1 in Eq. (5) except that elements of the stiffness matrix replace the longitudinal moduli:

$$C_1^* = \frac{1}{Q_{xx}^{(1)}} + \frac{1}{\lambda Q_{xx}^{(2)}} \tag{32}$$

and $\tau_i'(a)$ is the slope of the interfacial shear stress at the location of the microcrack. The equation defining $\tau_i'(a)$ is given in Ref. [61]. This analysis is again best characterized as a one-dimensional analysis with a minor correction for Poisson contraction. If we set $\nu_{xy}^{(i)}$ to zero, ϕ^2 reduces to

$$\phi^2 = \frac{C_1}{C_4} \tag{33}$$

which differs only by a numerical prefactor from the reduced Flaggs' result (see Eq. (29)). The fact that Nuismer and Tan's [61] analysis is the only one-dimensional analysis with a non-zero ω sets it apart from all other one-dimensional analyses. The consequence of a non-zero ω is discussed briefly later.

3.3.   Variational Mechanics of $[(S)/90_n]_s$ Laminates

The first two-dimensional analysis for the $x - z$ plane is derived by Hashin [65–68]. Hashin makes one and only one assumption — that the x-axis tensile stresses in each ply group depend only on x and are

independent of z. Under this assumption and force balance, the x-direction tensile stresses of a microcracked laminate, with the inclusion of thermal stresses, are [69]:

$$sxx1 = k_m^{(1)}\sigma_0 - \psi(x) \qquad \text{and} \qquad \sigma_{xx}^{(2)} = k_m^{(2)}\sigma_0 + \frac{\psi(x)}{\lambda} \tag{34}$$

where $\psi(x)$ is an undetermined function of x. By integrating the stress equilibrium equations and making use of boundary conditions, it is possible to express the shear and transverse stresses in terms of $\psi(x)$ [65, 66, 69]:

$$
\begin{aligned}
\sigma_{xz}^{(1)} &= \psi'(x)z & \sigma_{xz}^{(2)} &= \frac{\psi'(x)}{\lambda}(h - z) \\
\sigma_{zz}^{(1)} &= \frac{\psi''(x)}{2}(ht_1 - z^2) & \sigma_{zz}^{(2)} &= \frac{\psi''(x)}{2\lambda}(h - z)^2
\end{aligned}
\tag{35}
$$

where $h = t_1 + t_2$, $z = 0$ is at the midplane of the laminate, and Eq. (35) applies for $z \geq 0$ (the stresses for $z < 0$ follow by symmetry). As can be verified by substitution, the above stress state satisfies equilibrium, traction boundary conditions, and interface stress continuity, and is therefore an admissible stress state. By the principle of minimum complementary energy, the function $\psi(x)$ that minimizes the complementary energy gives the best approximation to the microcracked cross-ply laminate stress state. The complementary energy is minimized using the calculus of variations. Hashin solves the elastic problem [65, 66] and Nairn extends his result to include thermal stresses and more general mechanical properties [69]. The governing Euler equation for finding $\psi(\xi)$ is [69]

$$\frac{d^4\psi}{d\xi^4} + p\frac{d^2\psi}{d\xi^2} + q\psi = -k_{th}^{(1)}T \tag{36}$$

where $p = \frac{C_2 - C_4}{C_3}$, $q = \frac{C_1}{C_3}$, C_1 and C_4 are defined in Eqs. (5) and (30), and

$$C_2 = \frac{\nu_{xz}^{(1)}}{E_x^{(1)}}\left(\lambda + \frac{2}{3}\right) - \frac{\lambda\nu_{xz}^{(2)}}{3E_x^{(2)}} \tag{37}$$

$$C_3 = \frac{1}{60E_z^{(1)}}\left(15\lambda^2 + 20\lambda + 8\right) + \frac{\lambda^3}{20E_z^{(2)}} \tag{38}$$

The solution to Eq. (36) for the most common case of $4q/p^2 > 1$ is quoted from Ref. [69]:

$$\psi = \sigma_{x0}^{(1)}\phi(\xi) - k_{th}^{(1)}T \tag{39}$$

and

$$\sigma_{xx}^{(1)} = \sigma_{x0}^{(1)}(1 - \phi(\xi)) \tag{40}$$

where

$$
\begin{aligned}
\phi(\xi) = \ &\frac{2(\beta\sinh\alpha\rho\cos\beta\rho + \alpha\cosh\alpha\rho\sin\beta\rho)}{\beta\sinh 2\alpha\rho + \alpha\sin 2\beta\rho}\cosh\alpha\xi\cos\beta\xi \\
&+ \frac{2(\beta\cosh\alpha\rho\sin\beta\rho - \alpha\sinh\alpha\rho\cos\beta\rho)}{\beta\sinh 2\alpha\rho + \alpha\sin 2\beta\rho}\sinh\alpha\xi\sin\beta\xi\}
\end{aligned}
\tag{41}
$$

and

$$\alpha = \frac{1}{2}\sqrt{2\sqrt{q} - p} \qquad \text{and} \qquad \beta = \frac{1}{2}\sqrt{2\sqrt{q} + p} \tag{42}$$

The solution for $4q/p^2 < 1$ can be found in Refs. [55] and [69].

The x-axis tensile stress in the 90° plies and the interfacial shear and transverse stresses for a $[0/90_2]_s$ carbon/epoxy laminate are plotted in Fig. 9. The tensile stress $(\sigma_{xx}^{(1)})$ is qualitatively similar to the one-dimensional analysis result. It differs in detail by having zero slope at the microcrack surfaces and by reaching a different maximum stress midway between the microcracks. The interfacial shear stress is significantly different, especially on the microcrack surfaces. Unlike the one-dimensional analysis which has non-zero
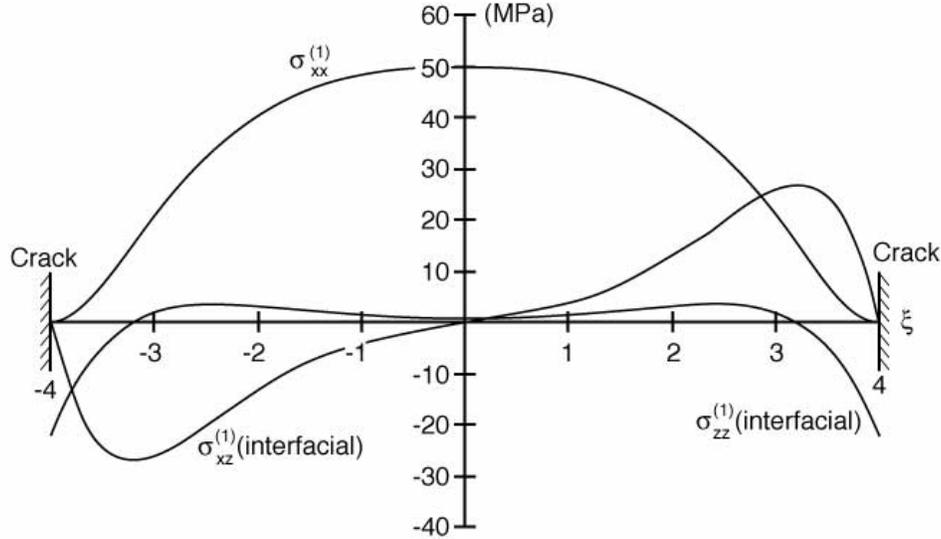
Fig. 9. Stresses between two microcracks in a $[0/90_2]_s$ carbon/epoxy laminate from the two-dimensional, variational mechanics analysis. The applied stress is 100 MPa, thermal load is $T = -125°C$, and the microcrack spacing is $\rho = 4$. The normal stress ($\sigma_{xx}^{(1)}$) is the average tensile stress in the 90° ply group. The plotted shear stress ($\sigma_{xz}^{(1)}$) and transverse stress ($\sigma_{zz}^{(1)}$) are the stresses at the 90/0 interface.

shear stress on the microcrack surfaces, the two-dimensional analysis satisfies the zero shear stress boundary condition. In addition, the two-dimensional analysis defines the transverse stress that remains undefined in all one-dimensional analyses. The transverse stress at the 90/0 interface is compressive near the microcrack tips and becomes slightly tensile away from the microcracks. The peak transverse stress in the $x - z$ plane is tensile and occurs at $z = 0$ or at the laminate midplane (plot not shown) [65, 66].

Hashin's [65, 66] variational mechanics analysis is based on an assumed stress field and minimum complementary energy. Fang *et. al.* [70] use assumed displacement fields and derive a variational mechanics solution by minimizing potential energy. Their displacement field, however, assumes zero z axis displacement. By our definition in this section, the Fang *et. al.* [70] analysis is a one-dimensional analysis. Although a direct comparison of their results to other one-dimensional analyses is difficult, their stress solutions, containing single $\sinh \phi\xi$ and $\cosh \phi\xi$ terms, are characteristic of one-dimensional solutions.

3.4. $[90_n/(S)]_s$ Laminates

The stress analysis of $[90_n/(S)]_s$ laminates is more complicated than the stress analysis of $[(S)/90_n]_s$ laminates. The major complicating feature is from the observation of a staggered microcracking pattern in the two 90° ply groups [22, 31, 32] (see Fig. 4B).

Because the one-dimensional analyses do not include transverse stresses, they make no distinction between $[(S)/90_n]_s$ and $[90_n/(S)]_s$ laminates. In other words, the one-dimensional solution to the stresses in $[(S)/90_n]_s$ laminates is simultaneously a solution to the stresses in $[90_n/(S)]_s$ laminates. This discloses a severe deficiency of all one-dimensional analyses. Experimental observations show that the microcracking properties of $[90_n/(S)]_s$ laminates differ from from those of $[(S)/90_n]_s$ laminates [15, 32]. It is clear that no one-dimensional analysis can predict the differences. As stated in the Introduction, a good micromechanics of damage analysis should be able to correlate data from a wide variety of laminates. By this criterion, it is not possible to construct a successful micromechanics of damage analysis for microcracking using a one-dimensional stress analysis.

In contrast, a two-dimensional analysis includes transverse stresses and might be able to explain the microcracking properties of $[90_n/(S)]_s$ laminates. Nairn and Hu [54] extend Hashin's [65, 66] two-dimensional, variational mechanics analysis to account for the staggered microcracks in $[90_n/(S)]_s$ laminates. We briefly describe the analysis results below. Details are given in Ref. [54].

The two 90° ply groups are labeled 1 and 4. By analogy with the analysis of $[(S)/90_n]_s$ laminates, it is assumed that after the formation of microcracks, the x-axis tensile stresses in the two 90° ply groups change to

$$\sigma_{xx}^{(1)} = k_m^{(1)}\sigma_0 - \psi_1(x) \qquad \text{and} \qquad \sigma_{xx}^{(4)} = k_m^{(4)}\sigma_0 - \psi_4(x) \tag{43}$$

For symmetric laminates $k_m^{(1)} = k_m^{(4)}$. When the microcrack in ply group 4 is midway between the microcracks in ply group 1 (*i.e.* perfect stagger, see Fig. 7A) symmetry dictates that

$$\psi_4 = \begin{cases} \psi_1(\xi - \rho) & \text{for } \xi > 0 \\ \psi_1(\xi + \rho) & \text{for } \xi < 0 \end{cases} \tag{44}$$

By virtue of Eq. (44), $\psi_1(x)$ and $\psi_4(x)$ are dependent functions. They can be treated as independent functions, however, if we consider them only on the interval $(0, \frac{\rho}{2})$, which is one quarter of the "unit cell" of damage, and impose appropriate boundary conditions at $\xi = 0$ and $\xi = \frac{\rho}{2}$ [54]. After these two independent functions on the interval $(0, \frac{\rho}{2})$ are obtained, the complete ψ_1 and ψ_4 functions can be constructed by symmetry and Eq. (44) [54]. The solution on the interval $(0, \frac{\rho}{2})$ is determined by minimizing the complementary energy using the calculus of variations. When cast in terms of two new functions

$$X = \psi_1 + \psi_4 \qquad \text{and} \qquad Y = \psi_1 - \psi_4 \tag{45}$$

the complementary energy can be minimized analytically by solving two decoupled fourth order differential equations (see Ref. [54]).

The x-axis tensile stress in the 90° plies (group 1) and the interfacial shear and transverse stresses for a $[90_2/0]_s$ carbon/epoxy laminate are plotted in Fig. 10. The tensile stress $(\sigma_{xx}^{(1)})$ is zero at the two microcrack surfaces as required by boundary conditions. Midway between the two microcracks and directly opposite the microcrack in the 90° ply group on the opposing surface (see Fig. 7A) there is a local minimum in tensile stress. This local minimum is caused by a bending effect resulting from the asymmetric nature of the unit cell of damage. Two local maxima in tensile stress are located at positions close to $\frac{1}{3}$ and $\frac{2}{3}$ of the way from the bottom microcrack to the top microcrack. The distribution of the tensile stress shown in Fig. 10 can be used to explain the tendency towards staggered microcracks. If new microcracks form at all local tensile stress maxima in the 90° plies, the new damage state is equivalent to three unit cells of damage each being $\frac{1}{3}$ as large as the initial unit cell of damage [54] (see Fig. 7B). Thus forming microcracks at positions of local maxima in tensile stresses leads to propagation of staggered microcracks.

As required by boundary conditions, the interfacial shear stress is zero on the microcrack surfaces. The shear stress is also zero at $\xi = 0$ due to symmetry. The peak shear stress is close to the microcrack surfaces and is similar in magnitude, but somewhat less than the peak $\sigma_{xx}^{(1)}$ stress.

$\sigma_{zz}^{(1)}$ plotted in Fig. 10 is the transverse stress along the 90/0 interface. There is a significant transverse stress concentration at the microcrack tip. The peak transverse stress is tensile and about twice as large as the peak $\sigma_{xx}^{(1)}$ stress. In dramatic contrast, the corresponding interfacial transverse stress in $[0/90_2]_s$ laminates shows a compressive stress concentration near the microcrack tips (see Fig. 9). The difference between $[90_2/0]_s$ and $[0/90_2]_s$ laminates in interfacial transverse stress is due to the bending effect caused by the asymmetric unit cell in $[90_2/0]_s$ laminates. It is the same bending effect that causes the local minimum in $\sigma_{xx}^{(1)}$. This high tensile transverse stress concentration is expected to promote mode I delamination initiating from the tips of microcracks. The difference in transverse tensile stresses between $[90_2/0]_s$ and $[0/90_2]_s$ laminates explain why, as observed by several authors [24, 32, 33, 47], delamination initiation occurs more easily in $[90_n/0_m]_s$ laminates than in $[0_m/90_n]_s$ laminates.

3.5. Finite Element Analysis

Finite element analysis is used to look at the stresses in the presence of microcracks (*e.g.* Refs. [25–28, 41, 71]) or in the presence of microcracks and delaminations (*e.g.* Refs. [27, 72, 73]). Used in this way, finite element analysis is a powerful tool for calculating the stresses in a model of a damaged laminate. It can, for example, be used to verify the accuracy of analytical methods such as the shear-lag analysis or the variational analysis. It can also be used to suggest the form of the correct solution and therefore be helpful in choosing approximations for new analytical solutions [54].
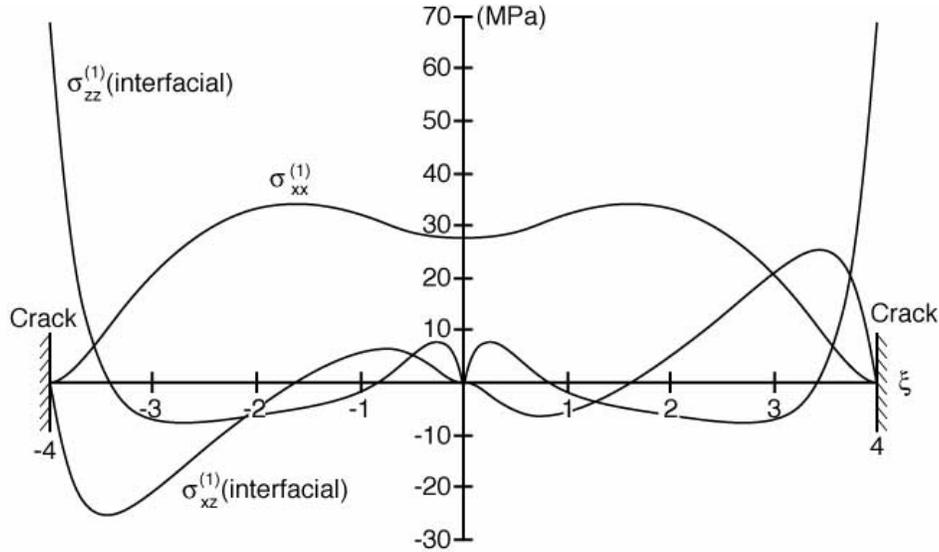
Fig. 10. Stresses between two microcracks in the 90° ply group of a $[90_2/0]_s$ carbon/epoxy laminate from a two-dimensional, variational mechanics analysis. The applied stress is 100 MPa, the thermal load is $T = -125°C$, and the microcrack spacing is $\rho = 4$. The normal stress $(\sigma_{xx}^{(1)})$ is for the entire ply group. The plotted shear stress $(\sigma_{xz}^{(1)})$ and transverse stress $(\sigma_{zz}^{(1)})$ are the stresses along the 90/0 interface.

Despite the important applications of finite element analysis, it is of limited use in developing useful micromechanics of damage models. Finite element analysis is best characterized as an experimental technique that can *measure* the stresses in model specimens. Even if the stress *measurement* is accurate, it is not sufficient for developing a micromechanics of damage model. A useful micromechanics of damage model requires knowledge of the stresses in the presence of any amount of damage and as a function of stacking sequence. Elucidating this information with finite element analysis may require hundreds of separate calculations. Thus, although finite elements could be used in principle, it is relatively intractable in practice. It is further unlikely that a finite element based micromechanics of damage model would find wide acceptance. It would be inhibited by the difficult task of transferring the methods from laboratory to laboratory. In this chapter, we limit our discussion of finite elements to information it gives about specific stress states or specific energy release rate calculations.

3.6. *Stress Analysis Predictions for Modulus Reduction*

As the density of microcracks increases, the longitudinal stiffness of the laminate decreases. At saturation microcrack density, the total modulus decrease ranges from about 5% to as much as 50% [65]. The maximum modulus reduction depends on laminate structure and material properties. Laminates whose axial stiffness is dominated by many 0° plies show a small modulus reduction. As the number of 90° plies increases and those plies play a greater role in the laminate stiffness, the laminate modulus reduction increases. The ratio of the transverse modulus to longitudinal (fiber direction) modulus of the unidirectional material is also important. The larger this ratio, the more the 90° plies contribute to laminate stiffness and therefore the larger the observed modulus reduction. To provide a critical test for theories that might predict modulus reduction, Highsmith and Reifsnider [22] did modulus reduction experiments on $[0/90_3]_s$ glass/epoxy laminates (Scotch Ply 1003). The $[0/90_3]_s$ stacking sequence was purposefully chosen to provide a laminate that is not dominated by the 0° plies. The ratio of the transverse modulus to longitudinal modulus of this glass/epoxy material is higher than it is for typical carbon/epoxy materials. The modulus reduction for glass/epoxy laminates is thus larger than it is for the corresponding carbon/epoxy laminate. In this section we compare Highsmith and Reifsnider's [22] experimental results — modulus as a function of microcrack density — with the predictions made by the one-dimensional analyses and by the two-dimensional, variational mechanics analysis.

From knowledge of the stress distribution, we can calculate the total displacement of the load bearing $0°$ plies between two microcracks using

$$u(P) = \int_{-a}^{+a} \varepsilon_{xx} dx = t_1 \int_{-\rho}^{+\rho} \left(\frac{\sigma_{xx}^{(2)}}{E_x^{(2)}} - \frac{\nu_{xz}^{(2)} \sigma_{zz}^{(2)}}{E_x^{(2)}} - \frac{\nu_{xy}^{(2)} \sigma_{yy}^{(2)}}{E_x^{(2)}} \right) d\xi \tag{46}$$

where P is applied load. In Eq. (46) we have ignored the displacement due to thermal expansion because for linear thermoelastic materials, the modulus is independent of the residual stresses. The compliance of the unit cell of damage is defined as

$$C = \frac{u(P) - u(0)}{P} \tag{47}$$

The effective modulus of the microcracked laminate follows by normalizing to the size of the unit cell

$$E = \frac{2a}{BWC} \tag{48}$$

We adopt a plane stress assumption in which $\sigma_{yy}^{(2)} = 0$, and the effective mechanical load constants, $k_m^{(1)}$ and $k_m^{(2)}$, are given by Eq. (3). Because there is no load applied in the thickness direction,

$$\int_{-\rho}^{+\rho} \sigma_{zz}^{(2)} d\xi = 0 \tag{49}$$

and thus for both one-dimensional and two-dimensional plane stress analyses the total displacement reduces to

$$u(P) = t_1 \int_{-\rho}^{+\rho} \frac{\sigma_{xx}^{(2)}}{E_x^{(2)}} d\xi \tag{50}$$

Inserting the one-dimensional stress in Eq. (20) results in

$$\frac{1}{E} = \frac{1}{E_c^0} \left(1 + \frac{E_x^{(1)}}{E_x^{(2)} \lambda \phi \rho} \tanh \phi \rho \right) - \frac{\omega(P) - \omega(0)}{E_x^{(2)} \phi^2 \sigma_0} \left(1 - \frac{\tanh \phi \rho}{\phi \rho} \right) \tag{51}$$

Most one-dimensional analyses have $\omega(P) - \omega(0) = 0$. For this special case, Eq. (51) reduces to

$$\frac{1}{E} = \frac{1}{E_c^0} \left(1 + \frac{E_x^{(1)}}{E_x^{(2)} \lambda \phi \rho} \tanh \phi \rho \right) \tag{52}$$

Substituting the two-dimensional, variational mechanics analysis results in [65, 66]:

$$\frac{1}{E} = \frac{1}{E_c^0} \left(1 + \frac{2 C_3 t_1 E_x^{(1)^2} \chi(\rho)}{B \rho} \right) \tag{53}$$

where $\chi(\rho)$ is a new function that physically corresponds to the excess strain energy in a "unit cell" of damage caused by the presence of microcracks. When $4q/p^2 > 1$

$$\chi(\rho) = 2\alpha\beta(\alpha^2 + \beta^2) \frac{\cosh 2\alpha\rho - \cos 2\beta\rho}{\beta \sinh 2\alpha\rho + \alpha \sin 2\beta\rho} \tag{54}$$

The $\chi(\rho)$ function for $4q/p^2 < 1$ is given in Ref. [69].

We substitute the various values of ϕ and $\omega(P)$ for the one-dimensional analyses and plot the modulus reduction in Fig. 11 together with the the modulus reduction predicted by the two-dimensional, variational mechanics analysis. The first and simplest one-dimensional analysis by Garrett and Bailey [11] is in excellent agreement with experimental observation. Later attempts for improved one-dimensional analyses generally give worse results. The analysis by Ogin *et. al.* [64], *i.e.*, the analysis that assumes parabolic displacements [45, 46, 58, 59, 64], under predicts the modulus reduction. In effect, the assumption of parabolic
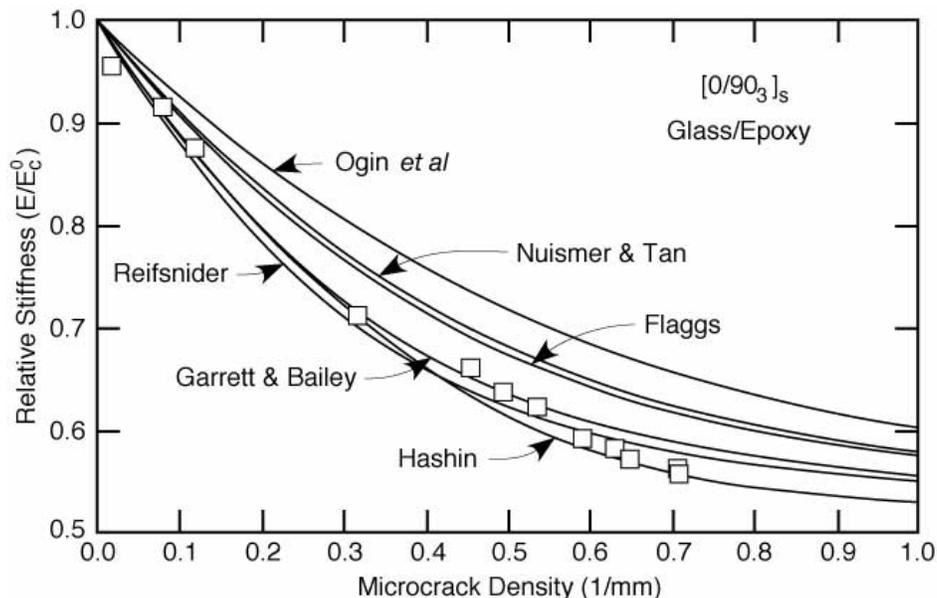
Fig. 11. Relative modulus as a function of microcrack density for a $[0/90_3]_s$ glass/epoxy (Scotch Ply 1003) laminate. The data points are experimental results from Ref. [22]. The smooth lines are theoretical predictions by various stress analysis procedures.

displacement makes the damaged $90°$ plies too stiff. Flaggs' shear-lag analysis [56] and Nuismer and Tan's elasticity analysis [61], which account for Poisson effects by including the y dimension, look better than the Ogin *et. al.* [45, 46, 64] analysis, but they are still too stiff and worse than Garrett and Bailey's [11] analysis. The non-zero $\omega(P)$ function in Nuismer and Tan's [61] analysis has little or no effect on the modulus reduction prediction. A plot with $\omega(P) = 0$ is indistinguishable from the Nuismer and Tan plot in Fig. 11. The Reifsnider type analysis, or a shear-lag analysis that uses an effective shear stress transfer layer [39, 57, 60] is in excellent agreement with experimental data. This excellent agreement, however, comes at the cost of using an adjustable parameter — G/t_0, the effective shear stiffness of the shear stress transfer layer. Overall, Hashin's [65, 66] variational mechanics analysis provides the best agreement with Highsmith and Reifsnider's [22] experimental observations. The improvement of Hashin's analysis over the best one-dimensional analysis, however, is only marginal.

Judged solely by their ability to fit the experimental data of Highsmith and Reifsnider [22], we should avoid the analyses that assume parabolic displacement and the quasi-two dimensional analyses of Flaggs [56] and Nuismer and Tan [61] as being too stiff. Of the remaining three analyses, we should also avoid the analysis that uses an effective shear stress transfer layer [39, 57, 60] i because it achieves agreement with experimental observations only by using an adjustable parameter that is not required in the other two analyses. Between the Garrett and Bailey [11] analysis and the Hashin [65, 66] analysis, we note that they have one assumption in common. The common assumption, which is the only assumption in the Hashin [65, 66] analysis, is that $\sigma_{xx}^{(i)}$ is independent of z. By the principles of variational mechanics, the Hashin [65, 66] analysis which minimizes complementary energy, is assured of finding the best approximation for all possible stress states with $\sigma_{xx}^{(i)}$ independent of z. We can thus conclude with mathematical rigor that the Hashin [65, 66] analysis is more accurate than the Garrett and Bailey [11] analysis.

Though necessary, an ability to fit the data of Highsmith and Reifsnider [22] is not sufficient to guarantee that a particular stress analysis is capable of providing a micromechanics of damage analysis for microcracking. The true test of any stress analysis is its ability to be used in conjunction with failure criteria to predict laminate failure properties. In the next section we explore the various failure models that have been proposed for predicting the initiation and propagation of microcracks. When we attempt to apply the failure criteria to make definite predictions, we do so by using the Hashin's [65, 66, 69] two-dimensional, variational mechanics analysis extended to include residual stresses. We find less incentive, except historical interest, to

explore the predictions made when using any one-dimensional analysis as we believe them to be less accurate than Hashin's [65, 66, 69] analysis.

4.   Failure Models

In the previous two sections, we discussed experimental observations on microcracking in $[(S)/90_n]_s$ and $[90_n/(S)]_s$ laminates and approximate stress analyses in the presence of microcracking damage. We are now in the position to explore micromechanics of damage models for microcracking. In this section we review the various failure criteria that have been proposed and use those criteria to make predictions about microcracking. By comparing the predictions with experimental observations we can critically evaluate various microcracking models.

4.1.   Microcrack Initiation in $[(S)/90_n]_s$ Laminates

Garrett and Bailey [11] assume that microcracking initiates when the x-direction stress in the $90°$ plies becomes equal to the transverse tensile strength of the unidirectional material. The theory simply states that microcracking initiates when

$$\sigma_{x0}^{(1)} = \sigma_T \tag{55}$$

where σ_T is the transverse tensile strength of a unidirectional laminate. Solving Eq. (55) for applied strain, we obtain the strain to initiate microcracking as

$$\varepsilon_{init} = \frac{\sigma_T - k_{th}^{(1)}T}{E_c^0 k_m^{(1)}} \tag{56}$$

where E_c^0 is the longitudinal modulus of the undamaged laminate. This analysis is a first-ply failure model derived using a maximum stress failure criterion.

Though simple in concept, the strength model or first-ply failure theory is in poor agreement with experimental observations. A straight forward experiment that demonstrates the poor agreement is to measure the stress to initiate microcracking for a series of laminates. If that stress is σ_{init}, we can calculate $\sigma_{x0}^{(1)}$ at the time of microcrack initiation using

$$\sigma_{x0}^{(1)} = k_m^{(1)}\sigma_{init} + k_{th}^{(1)}T \tag{57}$$

If the strength theory is valid, the calculated $\sigma_{x0}^{(1)}$ should be independent of laminate structure and for all laminates it should be equal to σ_T. The finding is that $\sigma_{x0}^{(1)}$ at microcrack initiation is strongly dependent on laminate structure [19, 42]. As the thickness of the $90°$ plies decreases, $\sigma_{x0}^{(1)}$ at microcrack initiation increases.

Crossman and Wang [42] recognize that $\sigma_{y0}^{(1)}$ at failure is also nonzero and that a simple strength criterion based solely on the magnitude of $\sigma_{x0}^{(1)}$ might be inadequate. To check for the possibility that more "sophisticated" failure criteria, such as quadratic failure criteria, might work better than the simple strength criterion, Crossman and Wang [42] measured both $\sigma_{x0}^{(1)}$ and $\sigma_{y0}^{(1)}$ at microcrack initiation. His finding is that no rational stress or strain based criterion can explain the dependence of microcrack initiation stress on laminate structure [42].

The only way a strength based micromechanics of damage analysis can work is if the transverse ply strength is treated is an *in situ* or laminate dependent property [19]. This approach, however, violates the principles of a good micromechanics of damage analysis outlined in the Introduction. We stated that a micromechanics of damage analysis should be definite enough that predictions can be made. Because a model that depends on *in situ* properties can not be used to make predictions, it is by definition *not* definite.

Some have argued that the strength model fails because a deterministic strength is used and that it should be replaced by a probabilistic or statistical strength model [19, 33, 34, 57, 74]. In support of a statistical strength model, we note that $\sigma_{x0}^{(1)}$ increases as the thickness of the $90°$ plies decreases. The increase in $\sigma_{x0}^{(1)}$ could be attributed to a size affect. Thinner $90°$ plies statistically have less flaws and therefore should have a higher effective strength. Two experimental observations, however, argue against using statistical strength

models. First consider microcracking in $[(S)/90_n]_s$ laminates *vs.* microcracking in $[90_n/(S)]_s$ laminates. The former fails by microcracking in a (90_{2n}) sublaminate while the latter fails by microcracking in two smaller (90_n) sublaminates. By the statistical strength theory, microcracking should form more easily in $[(S)/90_n]_s$ laminates than $[90_n/(S)]_s$ laminates. The experimental observation is just the opposite — the stress to initiate microcracking in $[90_n/(S)]_s$ laminates is lower than it is in $[(S)/90_n]_s$ laminates [15].

The second experimental observation discounting statistical strength theories is similar to the measurement of $\sigma_{x0}^{(1)}$ at microcrack initiation that discounts deterministic strength theories. The experiment is to assume that the transverse strength of the 90° plies follows a two-parameter Weibull distribution and measure those parameters for 90° plies in different laminates. The findings are that the Weibull parameters depend on the thickness of the 90° plies [19, 34]. Like the deterministic strength theories, the only way a statistical strength theory can work is if the distribution in transverse strength is treated as an *in situ* property. In short, statistical strength theories do not yield definite micromechanics of damage analyses that have predictive capabilities.

The failure of strength based models led Parvizi *et. al.* [13] to propose an energy criterion. They postulate that the first microcrack forms when the energy released due to the formation of that microcrack exceeds some critical value. If G_m is the energy release rate associated with the formation of a complete microcrack, the energy failure criterion is that a microcrack forms when $G_m \geq G_{mc}$. We call G_{mc} the microcracking fracture toughness or the intralaminar fracture toughness of the composite material system. Since the work of Parvizi *et. al.* [13], the energy criterion has gained popularity and appeared in Refs. [14–17, 24, 29–32, 54, 55, 58–60, 62, 69, 71].

To make predictions based on the energy criterion it is necessary to calculate the energy release rate associated with the formation of the first microcrack:

$$G_m = \frac{\partial \Omega}{\partial A} - \frac{\partial U}{\partial A} \tag{58}$$

where Ω is external work, U is internal strain energy, and A is fracture surface area. The formation of the first microcrack at constant load causes the total laminate displacement and internal strain energy to increase by Δu and ΔU respectively, and creates new fracture surface area $\Delta A = 2t_1 W$. The energy release rate due the formation of the first microcrack is

$$G_m = \frac{\sigma_0 B W \Delta u - \Delta U}{2t_1 W} \tag{59}$$

where σ_0 is the applied stress to initiate microcracking. It is certainly possible to calculate Δu and ΔU and therefore to calculate G_m from any approximate stress analysis. Many authors have given roughly equivalent results for G_m calculated from one-dimensional analyses [11–14, 24, 58, 59, 60, 62]. In view of the deficiencies in the one-dimensional analyses pointed out in the Stress Analysis section, however, the application of one-dimensional analyses to any failure criterion is only of historical interest. As previously stated, we concentrate on using Hashin's two-dimensional, variational mechanics analysis extended to include thermal stresses [65, 66, 69]. The variational mechanics analysis gives [75]:

$$G_m = 2\sigma_{x0}^{(1)^2}\alpha\sqrt{C_1 C_3} = \sigma_{x0}^{(1)^2} t_1 \sqrt{C_1\left(C_4 - C_2 + 2\sqrt{C_1 C_3}\right)} \tag{60}$$

where α is defined in Eq. (42).

By the energy criterion, the first microcrack forms when $G_m \geq G_{mc}$. Solving Eq. (60) for applied strain, we predict the strain to initiate microcracking as

$$\varepsilon_{init} = \frac{1}{k_m^{(1)} E_c^0} \left[\sqrt{\frac{G_{mc}}{t_1 \sqrt{C_1\left(C_4 - C_2 + 2\sqrt{C_1 C_3}\right)}}} - k_{th}^{(1)} T\right] \tag{61}$$

This prediction is in better agreement with experimental observation than any strength model because it correctly predicts that the strain to initiate microcracking increases significantly as the thickness of the 90° plies decreases [13, 75]. The agreement for laminates with very thick 90° plies is not as good. In general the

energy theory predicts that the strain to initiate microcracking decreases farther than what is experimentally observed [13]. Although the energy criterion is not a perfect failure criterion, it appears to capture most features of the experimental observations and to be a significant improvement over strength theories.

The inability of the energy criterion to fit all experimental microcrack initiation results may be related to deficiencies in the stress analysis (*e.g.* the assumption of constant x-direction tensile stress within ply groups). Alternatively, it may be due to practical problems associated with microcrack initiation experiments. In microcrack initiation experiments, one looks for the first microcrack and obtains only one data point per laminate. For imperfect laminates containing processing flaws, these types of experiments are inherently sensitive to flaws and perhaps even dominated by flaws. Because processing flaws do not enter the energy release rate calculation, none of the discussed theories can explain results that are influenced by processing flaws. Recent experimental evidence suggests that the first few microcracks are indeed associated with laminate flaws [29]. A typical result is shown in Fig. 3. The microcrack density for the $[0_2/90_4]_s$ laminate shows a characteristic rapid rise in microcrack density soon after the first few microcracks. The first few microcracks, however, appear at a stress below the predicted rapid rise in microcrack density. These early microcracks are noted to be near obvious processing flaws [29]. These comments imply that microcrack initiation experiments may not be the best experiments for studying the microcracking process. The preferred experiments are those that measure microcrack density as a function of applied load. In microcrack density experiments, one obtains many data points from a single laminate. If the first few microcracks are caused by laminate flaws, they can be ignored and many points still remain for studying the microcracking process. Although early microcracking investigations concentrated on microcrack initiation experiments, most recent studies involve microcrack density experiments.

4.2. Microcrack Density in $[(S)/90_n]_s$ Laminates

In microcrack density experiments, one measures the microcrack density as a function of applied load. The goal of micromechanics of damage analysis is to predict the experimental results. Hopefully the prediction can be applied to a variety of laminate structures and materials.

As with microcrack initiation experiments, the first attempt at predicting microcrack density experiments was a simple strength model [11]. From all stress analyses, the maximum tensile stress in the $90°$ ply group occurs midway between two existing microcracks at $\xi = 0$. The strength theory predicts that the next microcrack occurs when the longitudinal stress at $\xi = 0$ becomes equal to the transverse tensile strength of the unidirectional material, σ_T. Using the variational mechanics solution [65, 66, 69], the next microcrack occurs when

$$\sigma_T = \sigma_{x0}^{(1)}\big(1 - \phi(0)\big) \tag{62}$$

where $\phi(0)$ is defined in Eq. (41). Solving for applied stress, we predict the stress as a function of microcrack density to be

$$\sigma_0 = \frac{1}{k_m^{(1)}} \left(\frac{\sigma_T}{1 - \phi(0)} - k_{th}^{(1)} T \right) \tag{63}$$

If σ_T is treated as an adjustable parameter, the strength theory predictions are in reasonable agreement with experimental observations [11]. The problem with the strength theory is that fitting results from different laminate structures requires using different values of σ_T. In other words, the transverse tensile strength must be treated as an *in situ* or laminate dependent property. Several investigators try statistical strength theories for microcrack densities [20, 33, 34, 57, 74]. As in the simple strength model, however, the Weibull parameters must be treated as *in situ* or laminate dependent properties if one hopes to fit results for different laminates [34]. We thus conclude that micromechanics of damage models based on strength theories have little useful predictive capability.

Although energy release rate failure criteria were proposed for microcrack initiation in 1978 [13], it was not until 1986 that Caslini *et. al.* [24] suggested using total microcrack energy release rate to predict microcrack density as a function of applied load. The expression for energy release rate is given by Eq. (59). For any of the approximate stress analyses it is a straight forward matter to calculate W and U as functions of microcrack density. The less straight forward matter is how to evaluate the derivative terms $\frac{\partial W}{\partial A}$ and $\frac{\partial U}{\partial A}$. If D is the microcrack density, then the total microcrack fracture area is

$$A = 2t_1 W L D \tag{64}$$

Caslini *et. al.* [24] treat A as a continuous variable and use the one-dimensional analysis of Ogin *et. al.* [45, 46, 64] to derive a simple expression for G_m. Han *et. al.* [58, 59] use an identical stress analysis and a crack closure technique to derive an identical expression for G_m. Laws and Dvorak [60] recognize that A is not a continuous variable but changes in discrete steps of $\Delta A = 2t_1 W$ following the formation of each new microcrack. They advocate considering the formation of a new microcrack at a given microcrack density as a discrete process as illustrated in Fig. 6. The energy release rate for the formation of a complete microcrack is the difference in energy between the three microcrack state in Fig. 6B and the two microcrack state in Fig. 6A. Laws and Dvorak [60] calculate a discrete energy release rate using a one-dimensional analysis.

Nairn *et. al.* [29, 31, 69] calculate the microcracking energy release rate using Hashin's variational mechanics analysis extended to include thermal stresses [65, 66, 69]. Although most microcrack density analyses assume periodic arrays of microcrack spacing, the variational mechanics analysis can handle any distribution of microcrack spacings. Consider a specimen with N microcracks characterized by microcrack spacings ρ_1, ρ_2, ..., ρ_N. From the variational mechanics analysis the specimen compliance is [29, 69]:

$$C = C_0 + \frac{2C_3 t_1 L k_m^{(1)^2}}{B^2 W} \frac{\sum_{i=1}^{N} \chi(\rho_i)}{\sum_{i=1}^{N} \rho_i} \tag{65}$$

where $C_0 = L/BE_c^0 W$ is the compliance of the undamaged laminate and the function $\chi(\rho)$ was defined in Eq. (54). Nairn *et. al.* [29, 31, 69] derive an expression for G_m in terms of a derivative of the compliance:

$$G_m = \frac{B^2 W^2 \sigma_{x0}^{(1)^2}}{2 k_m^{(1)^2}} \frac{dC}{dA} \tag{66}$$

Evaluating $\frac{dC}{dA}$ by differentiating Eq. (65) results in the final energy release rate expression [29, 31, 69]:

$$G_m = \sigma_{x0}^{(1)^2} C_3 t_1 Y(D) \tag{67}$$

where $Y(D)$ is a function that depends on the microcrack density, $D = \frac{N}{L}$, or more formally on the complete distribution of microcrack spacing:

$$Y(D) = LW \frac{d}{dA} \frac{\sum_{i=1}^{N} \chi(\rho_i)}{\sum_{i=1}^{N} \rho_i} = \frac{d}{dD} \left(D \langle \chi(\rho) \rangle \right) \tag{68}$$

where $\langle \chi(\rho) \rangle$ is the average value of $\chi(\rho)$ over the N microcrack intervals.

To use Eq. (67), $Y(D)$ must be evaluated. Following Laws and Dvorak [60], Nairn *et. al.* [29, 31, 69] evaluate $Y(D)$ for the discrete process of forming a new microcrack at dimensionless position $\xi = 2\delta - \rho_k$ in the kth microcrack interval (see Fig. 6B). A discrete differentiation of Eq. (68) results in

$$Y(D) = \frac{\Delta D \langle \chi(\rho) \rangle}{\Delta D} = \chi(\rho_k - \delta) + \chi(\delta) - \chi(\rho_k) \tag{69}$$

During a typical experiment, one does not know where the next microcrack will form and therefore does not know ρ_k or δ. It is known, however that $[(S)/90_n]_s$ laminates tend to form regularly spaced microcracks, especially when microcrack density is high enough that processing flaws play no role. We thus might expect

$$\rho_k \approx \langle \rho \rangle \qquad \text{and} \qquad \delta \approx \frac{\langle \rho \rangle}{2} \tag{70}$$

where $\langle \rho \rangle$ is the average value of ρ_i. With these approximations

$$Y(D) \approx 2\chi(\langle \rho \rangle/2) - \chi(\langle \rho \rangle) \tag{71}$$

Liu and Nairn [29] note results that are sensitive to the distribution of microcrack spacings and thus Eq. (71) is sometimes an oversimplification. From Eq. (67) it can be calculated that the energy release rate is higher when the microcrack forms in a large microcrack interval than it is when it forms in a small
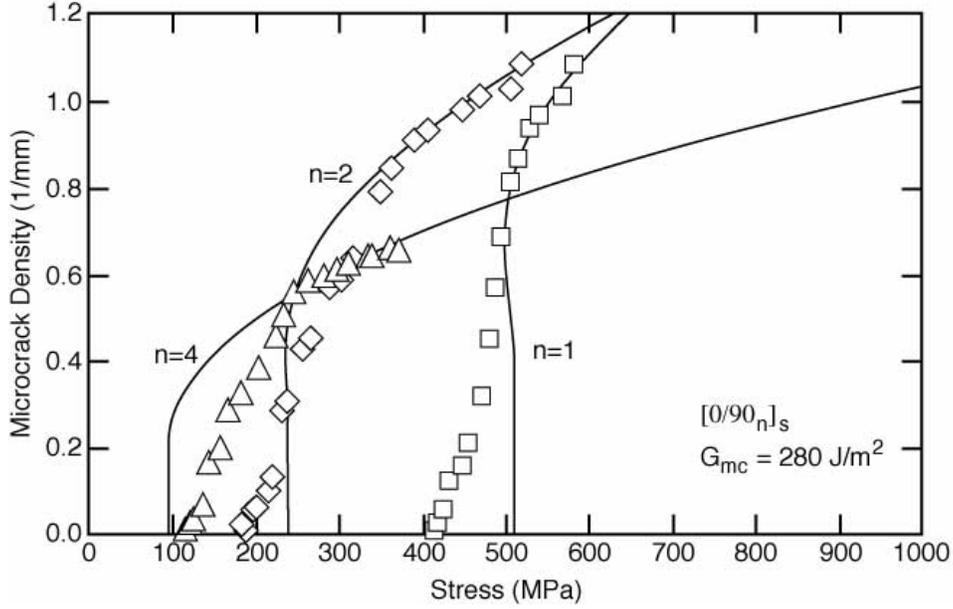
Fig. 12. Microcrack density as a function of applied load in a series of AS4/Hercules 3501-6 carbon/epoxy laminates. The symbols are experimental data points. The smooth lines are predictions using the variational mechanics energy release rate theory and $G_{mc} = 280$ J/m^2.

microcrack interval. If we assume that microcrack formation prefers locations that maximize energy release rate, then ρ_k will tend to be larger than $\langle\rho\rangle$ and δ will tend to be larger than $\frac{\langle\rho\rangle}{2}$. The best way to account for microcrack spacing distribution effects is to measure that distribution and calculate $Y(D)$ using Eq. (68). This approach is very tedious and Liu and Nairn [29] suggest a simpler approach that is in good agreement with experiments. Let the size of the microcrack interval where the new microcrack forms be a factor f times larger than the average microcrack interval. Then on average

$$\rho_k \approx f\langle\rho\rangle \qquad \text{and} \qquad \delta \approx \frac{f\langle\rho\rangle}{2} \tag{72}$$

which gives

$$Y(D) \approx 2\chi(f\langle\rho\rangle/2) - \chi(f\langle\rho\rangle) \tag{73}$$

Using f values between 1.0 and 1.44, Liu and Nairn [29] find good fits to results from a wide variety of laminates. Nairn and Bark [32] present an alternative approach based on the tedious process of measuring the distribution of microcrack spacings.

A rigorous test of the energy release rate theory requires experiments on many different laminate structures. Nairn and Bark [32] measured the microcrack density as a function of applied load in 20 different layups of AS4/Hercules 3501-6 carbon/epoxy laminates. We compare some of their results to predictions for experimental verification that the energy release rate theory predicts most of the microcracking properties of $[(S)/90_n]_s$ laminates. Solving Eq. (67) for applied stress, we obtain the stress as a function of microcrack density as

$$\sigma_0 = \frac{1}{k_m^{(1)}} \left(\sqrt{\frac{G_{mc}}{C_3 t_1 Y(D)}} - k_{th}^{(1)} T \right) \tag{74}$$

There is one unknown parameter in Eq. (74) — G_{mc}, the microcracking fracture toughness of the composite material system. For a single laminate, we can measure G_{mc} by fitting Eq. (74) to experimental results. If G_{mc} is a useful material property, however, it should be independent of laminate structure. If a single value of G_{mc} predicts the results from many different laminates, then we can claim experimental verification of a energy release rate micromechanics of damage model.
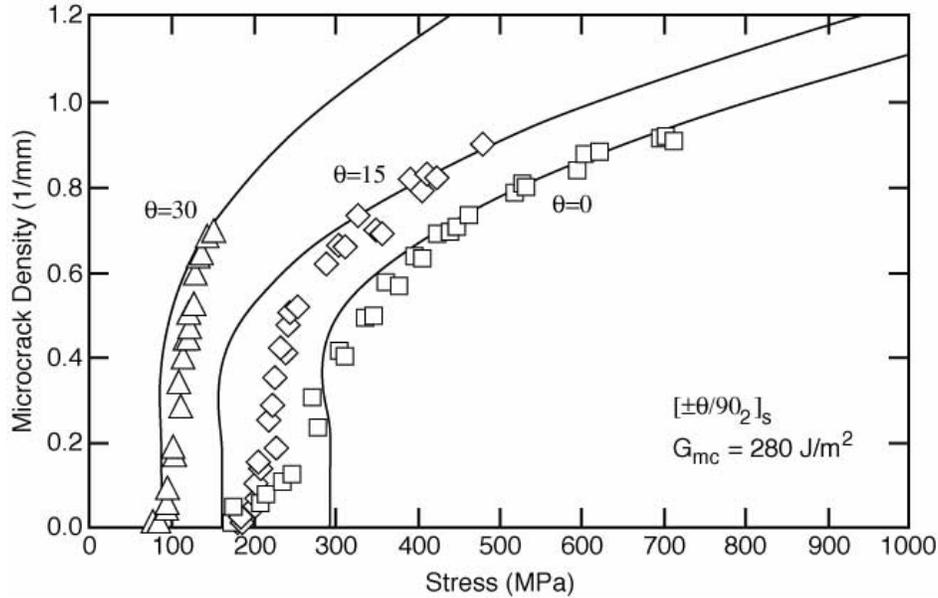
Fig. 13. Microcrack density as a function of applied load in a series of AS4/Hercules 3501-6 carbon/epoxy laminates. The symbols are experimental data points. The smooth lines are predictions using the variational mechanics energy release rate theory and $G_{mc} = 280$ J/m^2.

The results for $[0/90_n]_s$ laminates with $n = 1$, 2, and 4 are given in Fig. 12 [32]. All results are fit with a single value of $G_{mc} = 280$ J/m^2. As discussed later, this value of G_{mc} is similar, but slightly higher than the delamination or *interlaminar* fracture toughness of this material. The fits are good but we point out two deficiencies that should be the subject of future work. For $n = 4$ or for thick 90° ply groups, we consistently observe experimental results rising slower than predicted. This discrepancy could be associated with the approximate stress analysis that assumes the x-axis tensile stresses to be independent of z [65, 66, 69]. When the ply groups get thick, this approximation may be an oversimplification. For $n = 1$, a few microcracks start before the predicted rise in microcrack density. These early microcracks are probably associated with laminate flaws [29]. To account for these early microcracks, the energy theory needs to be modified to include laminate imperfections.

The results for $[\pm\theta/90_2]_s$ laminates with $\theta = 0°$, 15°, and 30° are given in Fig. 13 [32]. All results are predicted well at high microcrack density. There are some deviations at low microcrack density for $\theta = 15°$ that may warrant further investigation. The important feature is that these laminates are predicted with one value of $G_{mc} = 280$ J/m^2. In summary, Figs. 12 and 13 give results for six different $[(S)/90_n]_s$ laminates and all laminates are fit with one value of G_{mc}. The results for any individual laminate could be slightly improved by treating G_{mc} as an adjustable parameter, but doing that would violate the conditions for a fundamental micromechanics of damage model.

4.3.   *Simulation of Microcracking in $[(S)/90_n]_s$ Laminates*

In the early 1980's, prior to the suggestion of Caslini *et. al.* [24] that microcrack density is controlled by total energy release rate, Wang *et. al.* [25–28] described a computer simulation of microcracking in $[(S)/90_n]_s$ laminates. The simulation is stochastic in nature and attempts to account for laminate flaws. In brief, all laminates are assumed to have some distribution of effective flaws. As load increases, microcracks initiate when the largest flaw becomes critical. The critical load is calculated using fracture mechanics and an energy release rate that is calculated by a simple two-dimensional finite element analysis [25–28, 41, 71]. To predict microcrack density as a function of applied load, a Monte Carlo procedure is used. A series of laminates are generated in a computer having specific distributions of flaws. The specific flaw sizes and locations are generated from a four-parameter distribution of effective flaws. For each hypothetical laminate, the microcrack density as a function of applied load is calculated by determining when each specific flaw becomes

critical. Repeating this process for many hypothetical laminates gives a Monte Carlo simulation of microcrack density that can be fit to experimental results [25–28]. We believe there are important problems in Wang *et. al.*'s [25]wangd simulation that limit its usefulness as a micromechanics of damage model of microcracking. First, the two-dimensional finite element analysis oversimplifies the complex three-dimensional nature of real microcrack propagation. Wang *et. al.*'s [25–28] finite element analysis models microcrack propagation as proceeding in the z direction while experimental observations show that microcrack propagation is in the y direction [13]. Second, the four-parameter flaw distribution makes the analysis empirical. Like the strength models, the simulation process is not definite because it requires the flaw-distribution parameters to be laminate dependent, *in situ* parameters [25–28]. As discussed in the Introduction, micromechanics of damage models that are not definite can not make predictions and are therefore of limited use.

4.4.   *Microcracking in $[90_n/(S)]_s$ Laminates*

An important class of cross-ply laminates receiving significantly less study is laminates of generic layup $[90_n/(S)]_s$ or laminates having outer-ply 90° ply groups. As discussed earlier, the microcracking properties of $[90_n/(S)]_s$ laminates differ from those of the corresponding $[(S)/90_n]_s$ laminates. In particular, the initial microcracks form at lower loads in $[90_n/(S)]_s$ laminates and at saturation damage, the microcrack density of $[90_n/(S)]_s$ laminates is lower. Furthermore, $[90_n/(S)]_s$ laminates develop a staggered or antisymmetric pattern of damage (see Figs. 4 and 7) that complicates the stress analysis and the resulting micromechanics of damage analysis. In this section, we explore the use of an energy based micromechanics of damage model to predict the microcrack density as a function of applied load for $[90_n/(S)]_s$ laminates.

As explained in the Stress Analysis section, a one-dimensional analysis can not explain the observed differences between $[(S)/90_n]_s$ and $[90_n/(S)]_s$ laminates — we must use a two dimensional $x - z$ plane analysis. Nairn and Hu [54] extend Hashin's two-dimensional, variational mechanics analysis of $[(S)/90_n]_s$ laminates to $[90_n/(S)]_s$ laminates having staggered microcracks. They cast the solution in a form similar to the $[(S)/90_n]_s$ laminate analysis. The total energy release rate for the formation a new microcrack is expressed as

$$G_m = \sigma_{x0}^{(1)\,2} C_3 t_1 Y_a(D) \tag{75}$$

where $Y_a(D)$ is

$$Y_a(D) = LW \frac{d}{dA} \frac{\sum_{i=1}^N \chi_a(\rho_i)}{\sum_{i=1}^N \rho_i} = \frac{d}{dD}\Big(D\langle\chi_a(\rho)\rangle\Big) \tag{76}$$

Equations (75) and (76) are identical to the corresponding expressions for $[(S)/90_n]_s$ laminates (Eqs. (67) and (68)) except that $Y_a(D)$ and $\chi_a(\rho)$ replace $Y(D)$ and $\chi(\rho)$. The subscript a denotes laminates with antisymmetric or staggered microcracks. Physically $\chi_a(\rho)$ corresponds to the excess strain energy caused by the presence of staggered microcracks in a unit cell of damage of dimensionless spacing 2ρ (See Fig. 7). The function $\chi_a(\rho)$ is more complex than $\chi(\rho)$ and the reader is referred to Ref. [54] for details.

To test the microcracking analysis for $[90_n/(S)]_s$ laminates we compare the predictions to experimental results. The 20 layup study of microcracking in AS4/Hercules 3501-6 carbon/epoxy laminates includes $[90_n/(S)]_s$ laminates [32]. In fact, we have a more rigorous test for $[90_n/(S)]_s$ laminates than we did for $[(S)/90_n]_s$ laminates. The reason is that the results on $[(S)/90_n]_s$ laminates can be viewed as experiments that measured $G_{mc} = 280$ J/m². If Eq. (75) correctly accounts for outer-ply 90° plies and staggered microcracks, then it should be possible to fit experimental results for $[90_n/(S)]_s$ laminates with the same value of G_{mc}.

The results for $[90/0_n]_s$ laminates with $n = 0.5$, 1, 2, and 4 are given in Fig. 14. All results are fit with a single value of $G_{mc} = 240$ J/m². This microcracking fracture toughness is lower than the toughness used to fit the results for $[0_n/90_m]_s$ but close enough to be within experimental uncertainty. The fits for the $[90/0_n]_s$ laminates are better than the fits for the $[0_n/90]_s$ laminates. The results for $[90_2/\pm\theta]_s$ with $\theta = 0°$, 15°, and 30° are given in Fig. 15. These laminates are fit well with $G_{mc} = 280$ J/m². In summary, the microcracking properties of all AS4/Hercules 3501-6 laminates in Figures 12 to 15 can be predicted with an energy release rate based micromechanics of damage model and a microcracking toughness of $G_{mc} = 260 \pm 20$ J/m². The range of laminates that can be analyzed includes both $[(S)/90_n]_s$ laminates and $[90_n/(S)]_s$ laminates.
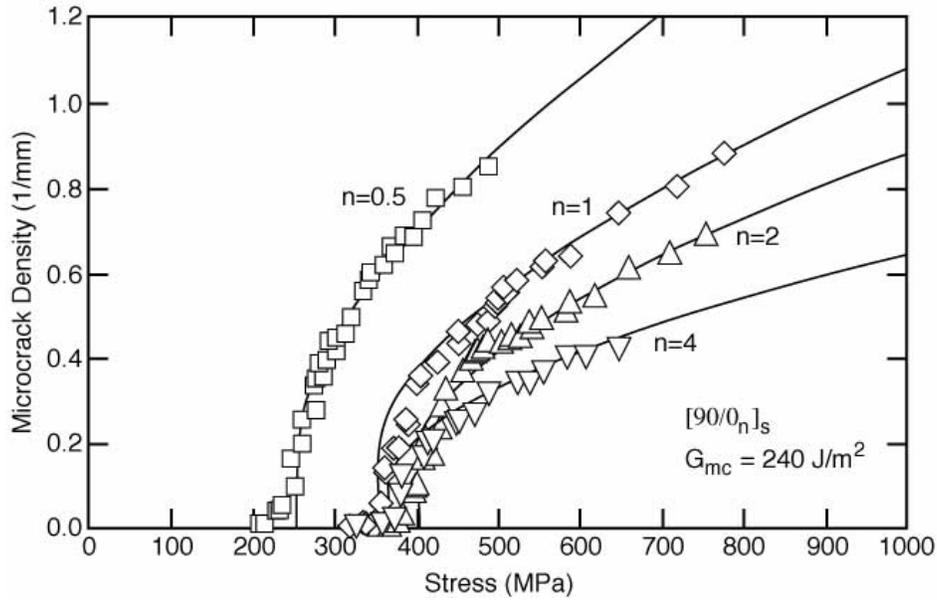
Fig. 14. Microcrack density as a function of applied load in a series of AS4/Hercules 3501-6 carbon/epoxy laminates. The symbols are experimental data points. The smooth lines are predictions using the variational mechanics energy release rate theory and $G_{mc} = 240 \ J/m^2$.
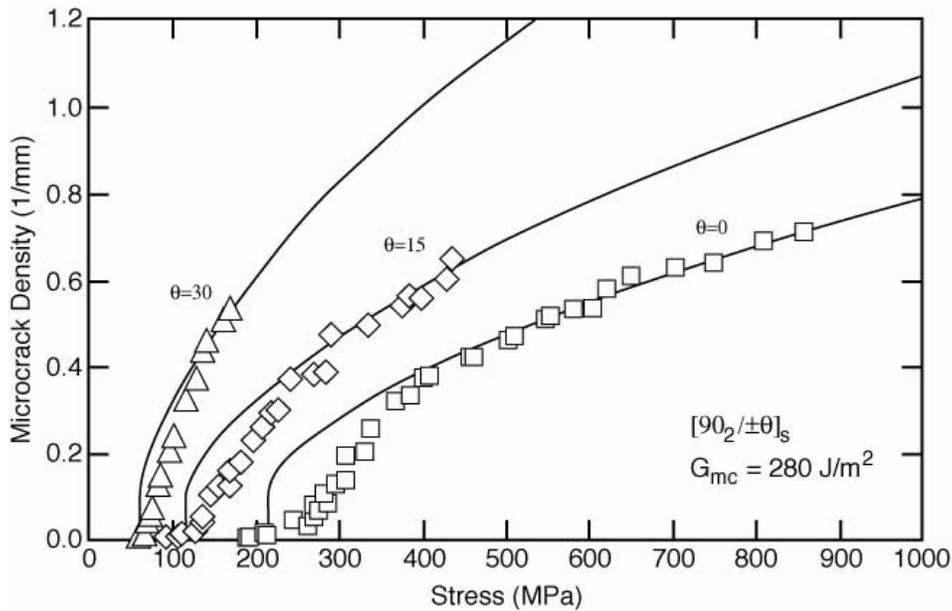

Fig. 15. Microcrack density as a function of applied load in a series of AS4/Hercules 3501-6 carbon/epoxy laminates. The symbols are experimental data points. The smooth lines are predictions using the variational mechanics energy release rate theory and $G_{mc} = 280 \ J/m^2$.

Table I. The microcracking fracture toughness, G_{mc}, of several composite material systems. All values of G_{mc} were determined from an energy release rate expression derived from a two-dimensional, variational mechanics analysis.

Material	G_{mc} J/m^2	Reference
AS4/Hercules 3501-6	230	30
AS4/Hercules 3501-6	240	29
AS4/Hercules 3501-6	260 ± 20	32
AS4/Dow Polycyanate	430	38
AS4/Dow Polycyanate	460	30
IM7/Hecules 8551-7	525	30
AS4/Dow Tactix$^\circledR$ 556	550	30
T300/Fiberite 934	690	29
G40-800/rubber modified Dow Polycyanate	720	38
AS4/Dow Tactix$^\circledR$ 696	825	30
IM6/DuPont Avimid$^\circledR$ K Polymer	960	29
T300/Fiberite 977-2	1800-2400	29
AS4/ICI PEEK	3000	29

5.   Further Results

The previous section showed that a micromechanics of damage model, based on total energy release rate for the formation of a complete microcrack, can explain many experimental observations. The best results are obtained by using Hashin's two-dimensional, variational mechanics analysis extended to include thermal stresses [65, 66, 69]. The two-dimensional analysis was required to be able to simultaneously predict results for both $[(S)/90_n]_s$ and $[90_n/(S)]_s$ laminates. In this section we apply the model to further failure problems.

5.1.   Microcracking Fracture Toughness

By analyzing microcrack density experiments it is possible to measure G_{mc}. Physically, G_{mc} is the energy required to form a complete microcrack or the microcracking fracture toughness. Because microcracks are within a ply group rather than between ply groups, G_{mc} is also an *intralaminar* fracture toughness. The higher the value of G_{mc} for a given composite material, the more resistant that material is to microcracking. In the previous section we showed that G_{mc} for AS4/Hercules 3501-6 carbon/epoxy laminates is 260 ± 20 J/m^2. Having established a method for measuring G_{mc}, it is useful to apply the technique to a variety of material systems.

Liu and Nairn [29], Yalvac [30, 38], and Nairn and Bark [32] measured G_{mc} for a variety of materials using the variational mechanics theory (*i.e.* the energy release rate in Eqs. (67) and (75)). The results are summarized in order of increasing toughness in Table I. The lowest toughness material is AS4/Hercules 3501-6. This material has been reported in three different references and G_{mc} is reproducibly 250 ± 30 J/m^2. The materials with tougher matrices than Hercules 3501-6 epoxy predictably have higher values of G_{mc}. Some examples include the toughened epoxies (IM7/Hercules 8551-7 and T300/Fiberite 977-2), the polycyanate matrices (AS4/Dow polycyanate and G40-800/rubber modified Dow polycyanate), and the thermoplastic matrices (IM6/duPont Avimid$^\circledR$ K Polymer and AS4/ICI PEEK). The G_{mc} for the toughened IM7/Hercules 8551-7 is double that of AS4/Hercules 3501-6 but similar in magnitude to other untoughened epoxy systems (e.g. T300/Fiberite 934). The G_{mc}'s for the two toughest materials (T300/Fiberite 977-2 and AS4/ICI PEEK) are based on only a few points and are regarded as approximate [29]. It was difficult to make these two toughest materials reliably microcrack during static loading [29].

The values of G_{mc} are qualitatively similar to delamination fracture toughness (G_{Ic}) measured using a double cantilever beam specimen. This correlation is expected because both microcracks and delamination are predominantly mode I crack growth through the matrix. The microcracking and delamination

processes differ in detail, however, because microcracking is an *intralaminar* process and delamination is an *interlaminar* process. For at least three materials (AS4/Hercules 3501-6, T300/Fiberite 934, and IM6/duPont Avimid®K Polymer) we have reliable results for both G_{mc} and G_{Ic}. In the two brittle epoxy materials, AS4/Hercules 3501-6 has $G_{mc} = 250$ J/m^2 and $G_{Ic} = 175$ J/m^2 [77], and T300/Fiberite 934 has $G_{mc} = 690$ J/m^2 and $G_{Ic} = 140$ J/m^2 [78]. In both cases G_{mc} is significantly larger than G_{Ic}. The implication is that cracks propagate more easily between plies than they do within a ply. The higher *intralaminar* toughness may be associated with increased fiber bridging during *intralaminar* fracture [76]. In the thermoplastic composite material (IM6/duPont Avimid®K Polymer), we find the opposite relation. For IM6/duPont Avimid®K Polymer $G_{mc} = 960$ J/m^2 and $G_{Ic} = 1200$ J/m^2 [76]. For this material, cracks propagate more easily within plies than between plies. The lower *intralaminar* fracture toughness may reflect the difficulty of achieving complete penetration of the thermoplastic matrix into the carbon fibers of each ply [76].

If G_{mc} is truly an *intralaminar* fracture toughness, then it should be expected to be nearly equal to the transverse fracture toughness of a unidirectional laminate. By transverse fracture toughness, we mean the fracture toughness of a through-the-thickness crack in a unidirectional laminate running parallel to the fibers but perpendicular to the plane of the plies. Although transverse fracture toughness is not commonly measured, it was recently measured for T300/Fiberite 934 and found to be 590 J/m^2 [78]. For T300/Fiberite 934, the microcracking fracture toughness ($G_{mc} = 690$ J/m^2) is much closer to the transverse toughness than it is to the delamination toughness.

5.2. *Mechanical and Thermal Fatigue*

Several investigators have measured the longitudinal stiffness of cross-ply laminates as a function of cycle number during constant amplitude load fatigue [22, 45, 46]. The goal is to assess the effect of fatigue loading on mechanical properties. Analyzing such fatigue data requires the simultaneous solution of two problems, which are the microcrack density as a function of cycle number and the effect of microcracks on mechanical properties. If attempts to fit experimental results fail, it may not be clear which problem introduces error. Even if data can be fit, it still may not be clear if the physics of the problem is understood or if there is nothing but a fortunate cancelation of error. The preferred approach is to separate these two problems. The effect of microcrack density on mechanical properties is a micromechanics problem that was discussed in the Stress Analysis section. The new problem is the prediction of the microcrack density as a function of cycle number during fatigue loading.

Liu and Nairn [44] suggest correlating fatigue data from numerous laminates by using a modified Paris Law [79] in which the microcrack density increase per cycle is given by

$$\frac{dD}{dN} = A\Delta G_m^n \tag{77}$$

where A and n are two power-law fitting parameters. From any laminate having 90° plies, it is a simple matter to calculate ΔG_m using Eq. (67) or Eq. (75). If Eq. (77) is valid, plotting dD/dN as a function of ΔG on a log-log plot should yield a linear relation. A problem with conventional Paris-law fatigue crack propagation experiments is that during the experiment, both the dependent variable (crack length) and the independent variable (ΔG or ΔK - stress intensity factor) change [79]. A fortunate feature of microcracking fatigue experiments, however, is that the calculated independent variable (ΔG) remains constant up to reasonably high microcrack densities. Figure 16 plots ΔG as a function of microcrack density for a typical fatigue experiment on a $[0_2/90_4]_s$ carbon/epoxy laminate. ΔG is constant up to a microcrack density of about 0.20 mm^{-1} and then drops rapidly to a lower value.

Some typical microcrack densities as a function of cycle number are shown in Fig. 16. At low microcrack density, where ΔG is constant, Eq. (77) predicts that microcrack density should increase linearly with cycle number (dD/dN = constant). The observation is that there is an initial rapid increase in microcrack density that is followed by a slower linear increase in microcrack density. In Fig. 16 the slower linear increase is from a microcrack density of 0.13 mm^{-1} to 0.23 mm^{-1}. Liu and Nairn [44] suggest that the initial rapid rise in microcrack density is due to laminate processing flaws and that the slower linear increase is a Paris-law region that characterizes the material's resistance for fatigue induced microcracking.
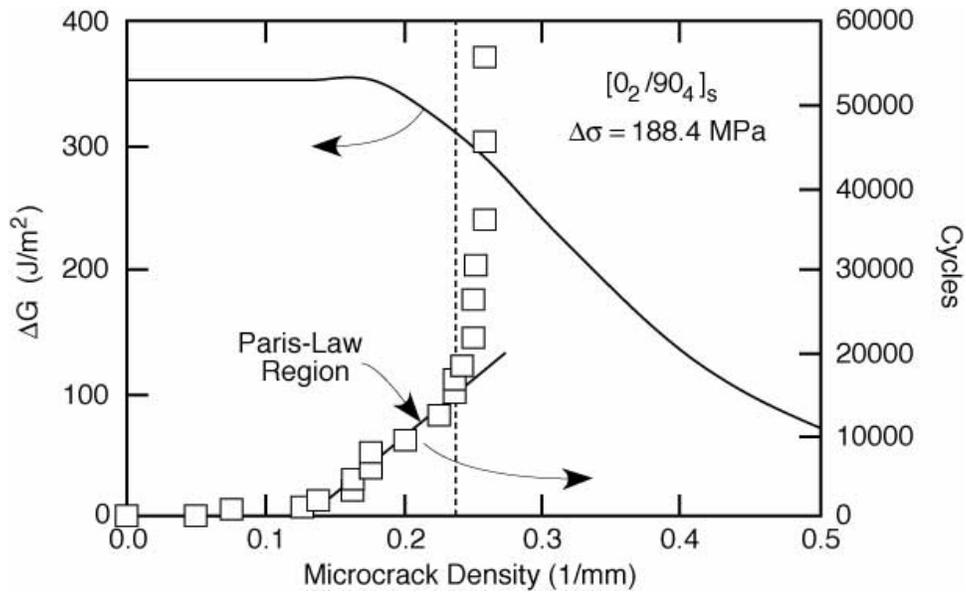
Fig. 16. Microcracking fatigue data for a $[0_2/90_4]_s$ carbon/epoxy laminate. The solid line shows ΔG as a function of microcrack density. The symbols show the microcrack density as a function of cycle number. The straight line through the microcrack density data shows the Paris-law region of constant microcrack density growth rate.
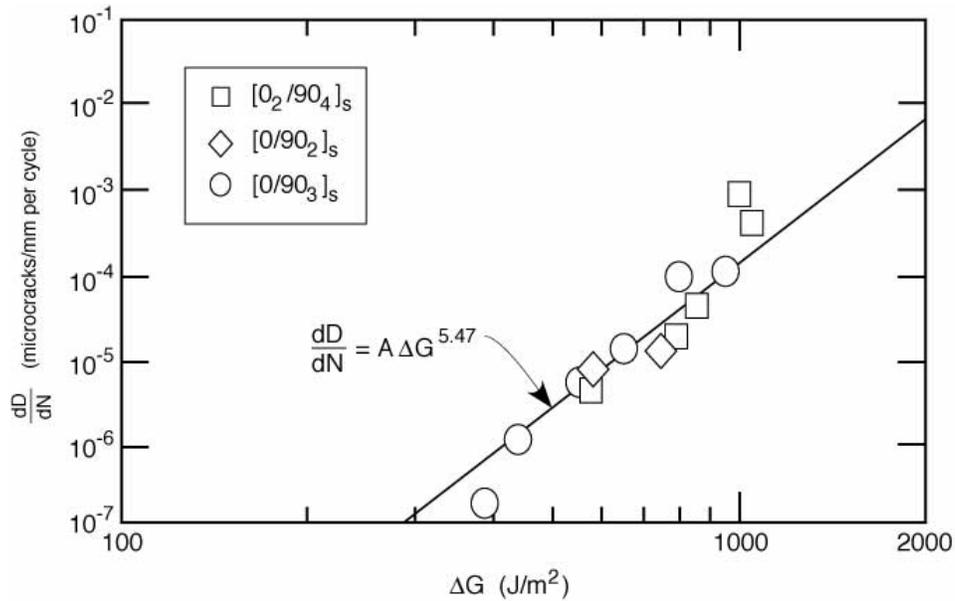

Fig. 17. The microcrack density growth rate (in microcracks per mm per cycle) as a function of applied ΔG for Avimid® K Polymer/IM6 laminates. As indicated on the figure, the results are from three different cross-ply layups.
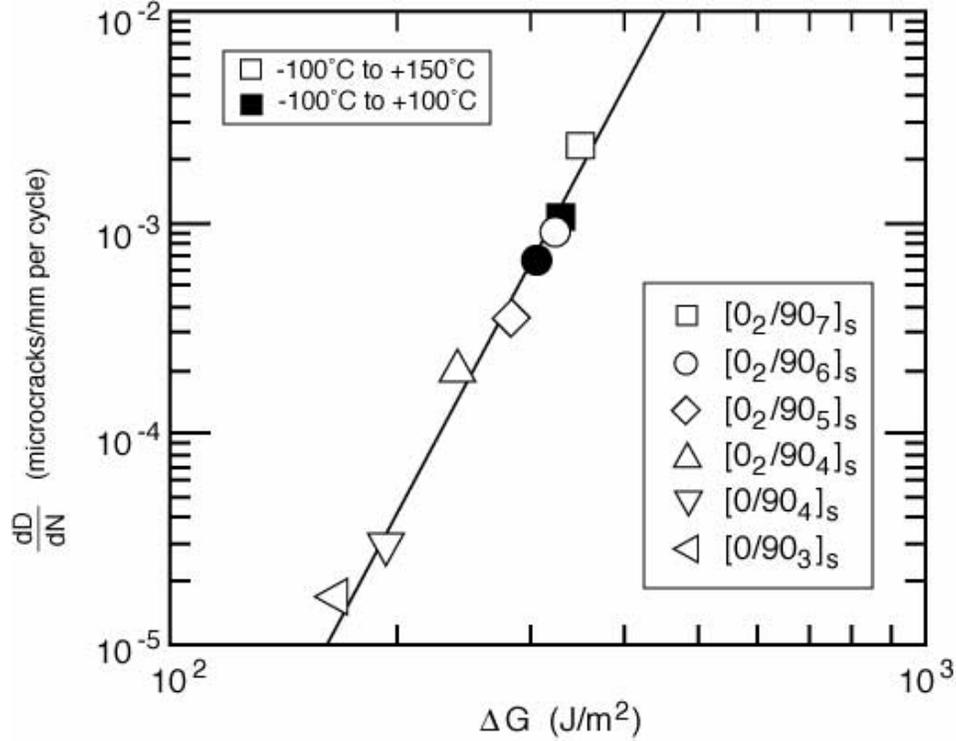
Fig. 18. The microcrack density growth rate (in microcracks/mm per cycle) as a function of applied ΔG for AS4/Hercules 3501-6 during thermal cycling. As indicated on the figure, the results are from six different cross-ply layups and from two different thermal cycling temperature ranges.

Two experimental observations support the use of the modified Paris-law in Eq. (77). First, the rate of increase in microcrack density dramatically decreases at a microcrack density similar to the point where ΔG begins to decrease (see Fig. 16). Second, Fig. 17 plots the slope of the Paris-law region defined in Fig. 16 as a function of ΔG for three different IM6/duPont Avimid® K Polymer laminates. The results for all laminates fall on a single master curve that is linear over a wide range in ΔG. The two points near $\Delta G = 1000$ J/m² deviate above the linear Paris-law line which indicates a rapid increase in microcrack density. A rapid increase in microcrack density at this level of ΔG is reasonable because the static microcracking toughness of this material is $G_{mc} = 960$ J/m² [29]. The lowest ΔG point deviates below the linear Paris-law and may be an indication of a threshold limit.

A similar Paris-law analysis can also be applied to thermal cycling fatigue experiments or to combined thermal and mechanical fatigue. Whatever the loading conditions are, Eqs. (67) and (75) can be used to calculate ΔG. For example, during thermal cycling

$$\Delta G = G_m(T_{min}) - G_m(T_{max}) \tag{78}$$

where T_{min} and T_{max} are the minimum and maximum temperatures of the thermal cycle. A typical Paris-law plot for thermal cycling experiments on AS4/Hercules 3501-6 laminates is in Fig. 18. The results in Fig. 18 are from six different $[0_n/90_m]_s$ laminates and the thermal cycling is between -100°C and +150°C or between -100°C and +100°C [44]. The fact that the results define a master Paris-law line supports the use of a Paris law in the analysis of thermal cycling experiments. Liu and Nairn [44, 80] attempted to correlate thermal cycling fatigue experiments with mechanical fatigue experiments and find the master Paris-law curves to be different. A possible explanation is that the during thermal cycling, microcracks form at the point of the highest thermal stress which occurs at the minimum temperature. If the fracture and mechanical properties are temperature dependent, which is likely true, it is reasonable to expect that thermal cycling fatigue properties will differ from room temperature mechanical fatigue properties.

5.3. Delamination

Considering the importance of delamination damage, the efforts aimed at explaining microcrack induced delaminations are limited. O'Brien [81, 82] developed the first analytical method for the energy release rate associated with the growth of microcrack induced delaminations by using simple load sharing rules and ignoring residual stresses. In regions adjacent to delaminations, the 90° plies are assumed to carry no load and thus the uncracked plies carry proportionately increased loads. In regions where there is no delamination, the stresses in all plies are identical to the stresses in the undamaged state. The resulting energy release rate is [81, 82]:

$$G_d = \frac{\sigma_0^2 B^2}{4} \left(\frac{1}{2t_2 E_x^{(2)}} - \frac{1}{BE_c^0} \right) \tag{79}$$

where subscript d denotes delamination. This G_d is independent of delamination size and is shown in subsequent calculations to be in reasonable agreement with three-dimensional finite element analysis [72]. Because stresses in regions where there is no delamination are assumed to be the same as that of the undamaged laminate, O'Brien's result is a limiting special case that applies to delaminations induced by isolated microcracks [55]. Experimental observations show that microcrack induced delaminations usually do not appear until after the formation of many microcracks [26, 40]. Thus, instead of analyzing delaminations induced by isolated microcracks, it is important to consider delaminations induced by microcracks in the proximity of neighboring microcracks.

Dharani and Tang [83] describe a consistent shear-lag theory analysis for both microcracking and microcrack induced delaminations. They predict failure using numerical stress calculations and a point-stress failure criterion. Many of their predictions are in qualitative agreement with experimental results. Like O'Brien's analysis [81, 82], however, Dharani and Tang's delamination study is limited to delamination at isolated microcracks.

Several authors carry out three-dimensional finite element analyses for free-edge and microcrack induced delaminations [27, 72, 73]. Fish and Lee [73] consider delaminations near the free edge that are inclined 45° with respect to the microcrack. The crack shape they assume is reasonable for free-edge delaminations in the absence of microcracks but is not a good representation of microcrack induced delaminations (see Refs. [26] and [40]). Wang *et. al.* [27] assume a specific delamination growth process and calculate the energy released as the delamination grows. Because they assume a specific growth process, their results are only useful in a qualitative sense. Salpekar and O'Brien [72] present the most comprehensive results including 45° inclined crack fronts, 10.6° inclined crack fronts, and through-the-width delaminations. They calculate mode I, mode II, and mode III energy release rates as functions of position along the various crack fronts. In general, the three-dimensional finite element analyses provide important information about edge effects that can not be learned from two-dimensional analyses. Their practical utility is limited, however, because by restricting the models to isolated microcracks they fail to account for the effect of neighboring microcracks.

Nairn and Hu [55] extend Hashin's two dimensional, variation mechanics analysis to account for delaminations emanating from microcrack tips. Figure 19 shows two microcracks having delaminations of length d_1 and d_2 emanating from the top and bottom microcrack tips. Applying Hashin's [65, 66] only assumption that $\sigma_{xx}^{(i)}$ is independent of z, the stresses in regions I and III of Fig. 19 reduce to a simple stress state. The 90° plies carry no load and the (S) sublaminate carries the load lost by the 90° plies in simple uniaxial tension. In regions I and III, the stresses reduce to [55]:

$$\sigma_{xx}^{(1)} = 0 \qquad\qquad \sigma_{xx}^{(2)} = \sigma_{x0}^{(2)} + \frac{\sigma_{x0}^{(1)}}{\lambda} = \frac{1+\lambda}{\lambda}\sigma_0$$

$$\sigma_{xz}^{(1)} = \sigma_{zz}^{(1)} = 0 \qquad \sigma_{xz}^{(2)} = \sigma_{zz}^{(2)} = 0 \tag{80}$$

In region II the stresses are identical to the stresses that exist between two microcracks separated by a dimensionless half spacing of $\rho - \delta$ where

$$\delta = \frac{d_1 + d_2}{2t_1} \tag{81}$$

Consider a sample having N microcrack intervals characterized by dimensionless spacings ρ_1, ρ_2, ..., ρ_N and dimensionless delamination lengths δ_1, δ_2, ..., δ_N. Nairn and Hu [55] use the new two-dimensional,
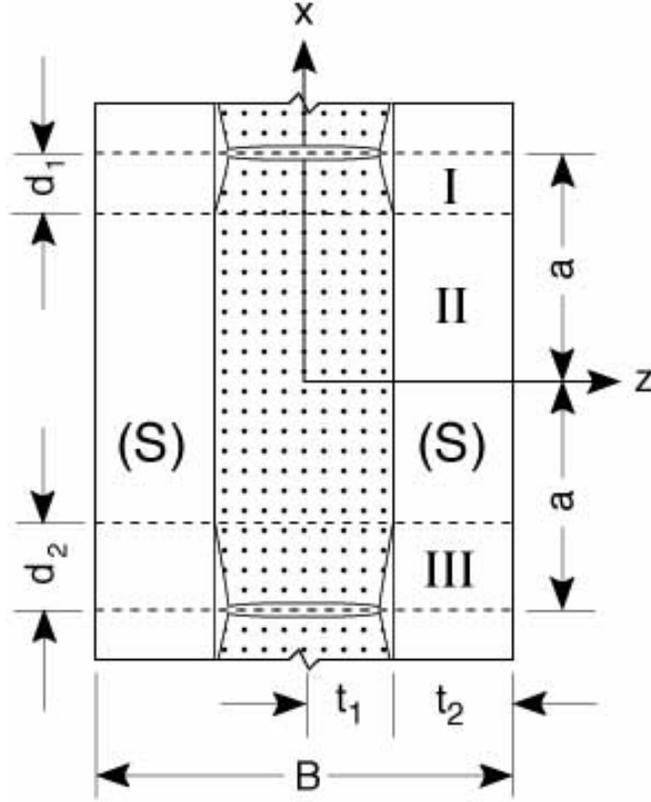
Fig. 19. Edge view of a $[0_n/90_m]_s$ cross-ply laminate with microcracks and delaminations emanating from the tips of those microcracks. The dashed lines demarcate regions I, II, and III for the stress analysis.

variational mechanics stress analysis to find the sample compliance:

$$C = C_0 + \frac{2t_1 E_x^{(1)^2}}{B^2 W E_c^{0^2}} \left(C_3(L-d) \frac{\sum \chi(\rho_i - \delta_i)}{\sum(\rho_i - \delta_i)} + C_1 d \right) \tag{82}$$

where d is the sum of the lengths of all delaminations. The energy release rate for the growth a single through-the-width delamination in microcrack interval k is [55]:

$$G_d = \sigma_{x0}^{(1)^2} C_3 t_1 \frac{\chi'(0) - \chi'(\rho_k - \delta_k)}{2} \tag{83}$$

The same $\chi(\rho)$ function that appears in the energy release rate expression for microcrack formation (see Eq. (67)) now appears differentiated in the energy release rate expression for delamination. Unlike O'Brien's [81, 82] simple result, the G_d in Eq. (83) depends on delamination size through δ_k. Taking the limit of G_d in Eq. (83) as $\rho \to \infty$ and setting $T = 0$ gives a result which is the energy release rate for growth of a delamination from isolated microcracks; the result is identical to O'Brien's [81, 82] result. The variational mechanics analysis of Nairn and Hu [55] can be viewed as a correction to O'Brien's [81, 82] result to account for microcrack growth in small microcrack intervals and to account for thermal stresses.

The variational mechanics delamination analysis can be used to discuss competition between microcracking and delamination. The first form of damage in cross-ply laminates is usually microcracking. Once the first microcrack has formed, we can ask if a delamination will initiate at that microcrack or if instead another microcrack will form. Comparing the energy release rate expression for microcracking (Eq. (67)) to the one for delamination (Eq. (83)), the predicted failure mode depends on the values of G_{mc} and G_{dc} (the delamination fracture toughness) and on the relative magnitudes of $2\chi(\rho/2) - \chi(\rho)$ and $\frac{1}{2}(\chi'(0) - \chi'(\rho))$. Assuming G_{mc} and G_{dc} are the same (they both represent crack growth through the matrix, albeit possibly
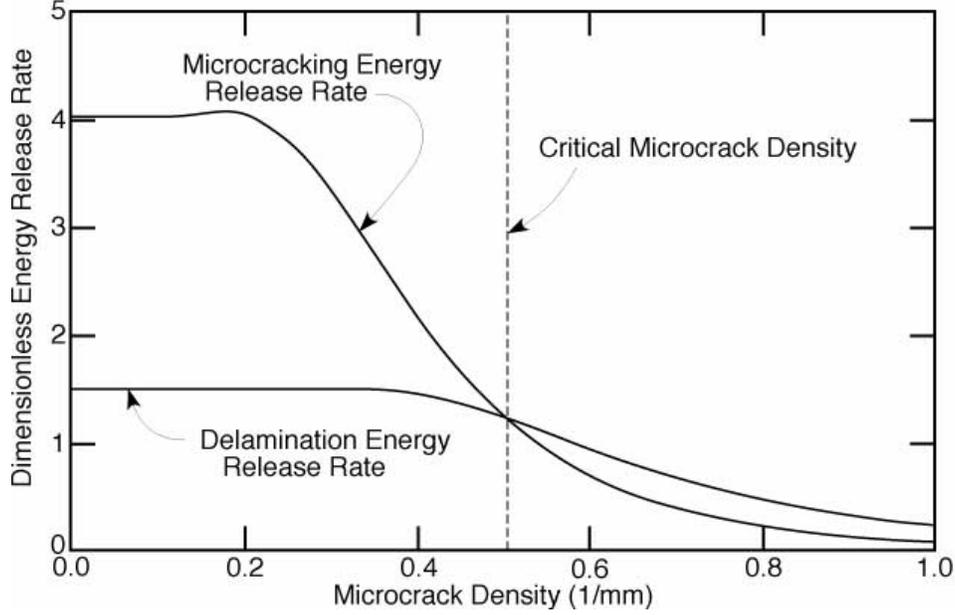
Fig. 20. Dimensionless energy release rates for initiation of delamination and for continued microcracking as functions of microcrack density for a $[0_2/90_4]_s$ carbon/epoxy laminate. The critical microcrack density for delamination is defined by the microcrack density where the two curves cross.

by different fracture modes — mode I *vs.* mode II), the predicted failure mode can be determined by plotting the latter two quantities. In Fig. 20, $2\chi(\rho/2) - \chi(\rho)$ and $\frac{1}{2}\left(\chi'(0) - \chi'(\rho)\right)$ or dimensionless energy release rates are plotted for a typical $[0_2/90_4]_s$ carbon/epoxy laminate.

Fig. 20 shows that at low microcrack densities, microcracking is the preferred mode of failure. At some critical microcrack density (0.51 mm^{-1} in Fig. 20), however, the energy release rate for a through-the-width delamination surpasses the energy release rate for microcracking and delaminations are expected to initiate at the microcrack tips. Once delaminations initiate, microcracking will cease and the delaminations will dominate failure. The critical microcrack density for delamination depends on the laminate structure. In agreement with experimental observations [26, 40], the more 90° plies, the lower the critical microcrack density for delamination. In other words, delaminations initiate more easily from microcrack tips in thick 90° ply groups. The critical microcrack density is virtually independent of the sublaminate (S) supporting the 90° plies [55]. Although sublaminate (S) has little effect on critical microcrack density, it has a significant effect on the load at which the critical microcrack density is reached. The stiffer the sublaminate (S), the higher the load required to reach a given microcrack density [29, 32].

Although we previously assumed that $G_{mc} = G_{dc}$, the conclusions drawn from Fig. 20 are easily generalized for $G_{dc} \neq G_{mc}$. We merely need to normalize the dimensionless energy release rates by dividing them by the critical energy release rates. The trends in the dimensionless energy release rates remain the same but one of them (*e.g.* the microcracking energy release rate) moves up or down relative to the other, depending on $G_{mc} < G_{dc}$ or $G_{mc} > G_{dc}$. Consequently the critical microcrack density increases (for $G_{mc} < G_{dc}$) or decreases (for $G_{mc} > G_{dc}$). In the limit of low delamination fracture toughness, the formation of the first microcrack might be immediately followed by initiation of delamination.

Experimental observations indicate that delamination and its propagation is not through-the-thickness [26, 40]. The delamination analysis problem is thus not two-dimensional. Nairn and Hu [55] construct a quasi-three dimensional analysis using an array of parallel, two-dimensional springs. They predict that a delamination that initiates at a free edge will propagate along the microcrack edge which is in the laminate width (y) direction [55]. There is less driving force for a delamination to propagate in the x direction. The sketches of predicted delamination growth in Ref. [55] are agree with sketches of experimentally observed delamination growth in Refs. [26] and [40].

The delamination analysis and predictions discussed above are for $[(S)/90_n]_s$ laminates or laminates with

interior 90° plies. Experimental observations show that laminates with microcracks in outer-ply 90° plies (e.g. $[90_n/(S)]_s$ laminates) are more susceptible to microcrack induced delaminations than the corresponding $[(S)/90_n]_s$ laminate [24, 32, 33, 47]. A recent variational mechanics analysis of $[90_n/(S)]_s$ laminates [54], explains this increased tendency towards delamination by noting that the asymmetry of the characteristic damage state leads to a bending effect that enhances the mode I character of the delamination process. No one has been able to analytically calculate the energy release rate for delamination in $[90_n/(S)]_s$ laminates. Work in progress shows that the two-dimensional, variational mechanics analysis of $[90_n/(S)]_s$ laminates can be extended to account for delaminations [84].

5.4. *Curved Microcracks*

At low microcrack densities microcracks in $[(S)/90_n]_s$ laminates are straight. The tendency towards periodic arrays of straight microcracks implies that new microcracks form approximately midway between existing microcracks. At high microcrack densities curved microcracks that make an angle of 40-50° with respect to the $90/(S)$ interface (see Fig. 4C) are observed [11, 14, 23, 37, 35]. Curved microcracks are always associated with existing straight microcracks and form at a position about one-ply thickness away from the straight microcrack [35, 37]. Groves *et. al.* [37] describe the only attempt at understanding the mechanism behind curved microcracks. They tried many failure criteria and postulate that curved microcracks form at local maxima in principle stress and that the curvature of the microcracks is determined by the trajectory of the maximum principle stress [37]. Their claims are qualitatively supported by finite element calculations that show a maximum in principle stress near existing straight microcracks that occurs near the $90/(S)$ interface. In agreement with experimental observation, the principle stress trajectories at the location of maximum principle stress make an angle of 40-60° with respect to the $90/(S)$ interface [37]. The location of the principle stress maximum, however, is only in qualitative agreement with experimental observations. The finite element analysis results show that the maximum principle stress is closer to the straight microcrack than the initiation site of experimentally observed curved microcracks [37].

It is interesting to apply Hashin's [65, 66, 69] two-dimensional, variational mechanics analysis to the prediction of curved microcrack formation using the maximum principle stress model proposed by Groves *et. al.* [37]. There are two goals to this exercise. First, if successful, we have further evidence that the stress components of Hashin's two-dimensional analysis are of sufficient accuracy for the basis of micromechanics of damage models. Second, we can derive analytical tools that might be useful in understanding curved microcracks.

In the $x - z$ plane, the maximum principle stress is

$$\sigma_{max} = \frac{\sigma_{xx} + \sigma_{zz}}{2} + \sqrt{\left(\frac{\sigma_{xx} - \sigma_{zz}}{2}\right)^2 + \sigma_{xz}^2} \tag{84}$$

Applying the two-dimensional, variational mechanics stress state for the 90° plies of $[(S)/90_n]_s$ laminates in Eqs. (34) and (35) gives

$$\sigma_{max} = \frac{k_m^{(1)}\sigma_0 - \psi(x) + \frac{\psi''(x)}{2}(ht_1 - z^2)}{2} + \sqrt{\left(\frac{k_m^{(1)}\sigma_0 - \psi(x) - \frac{\psi''(x)}{2}(ht_1 - z^2)}{2}\right)^2 + \psi'(x)^2 z^2} \tag{85}$$

Plotting Eq. (85) over the entire 90° ply group shows that the maximum principle stress always occurs at the $90/(S)$ interface, but its location on the interface depends on the microcrack density and on laminate structure [85]. Figure 21 plots the maximum principle stresses along the 90/0 interface of a $[0/90_2]_s$ carbon/epoxy laminate for four different microcrack densities. For low microcrack densities ($\rho \geq 3.0$ in Fig. 21) there is a broad maximum in principle stress midway between the two existing microcracks. The principle stress trajectory midway between two existing microcracks is normal to the 90/0 interface. The prediction is that only straight microcracks form when the microcrack density is low. At high microcrack densities ($\rho \leq 2.0$ in Fig. 21) there are two local maxima in principle stress. In agreement with experimental observations, the local stress maxima are approximately one to two ply thicknesses away from the existing microcracks. The location of the principle stress maxima is in better agreement with experimental observation than the finite element calculations by Groves *et. al.* [37]. We are enlightened by Fig. 21 that for any laminate structure
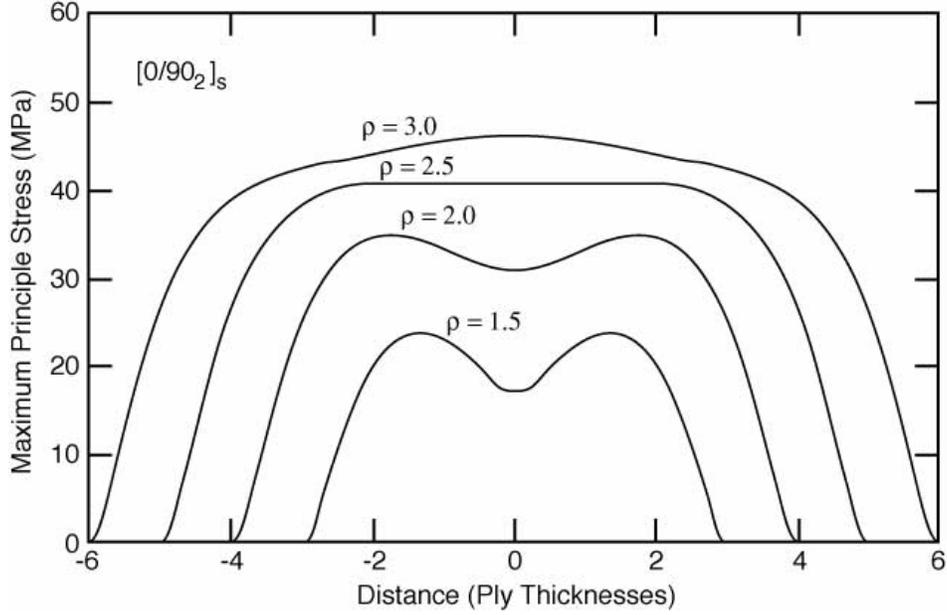
Fig. 21. The maximum principle stresses along the 90/0 interface in a $[0/90_2]_s$ carbon/epoxy laminate for four values of the microcrack density.

there is some critical microcrack density where the local principle stress maxima near existing microcracks are equal to the local principle stress maximum midway between existing microcracks. For the laminate in Fig. 21 the critical microcrack density is when $\rho = 2.0$. When the microcrack density is below the critical microcrack density, straight microcracks midway between existing microcracks will dominate. When the microcrack density is above the critical microcrack density, curved microcracks near existing straight microcracks will dominate.

Groves *et. al.* [37] suggest that the shape of curved microcracks can be approximated by the trajectory of the maximum principle stress that exists before the curved microcrack forms. This simple suggestion ignores the effect that a propagating curved microcrack has on principle stress trajectories, but it appears to be qualitatively correct [37]. The maximum principle stress trajectory in the $x - z$ plane can be determined from the differential equation

$$\frac{dz}{dx} = \frac{\sigma_{xx} - \sigma_{zz}}{2\sigma_{xz}} + \sqrt{\left(\frac{\sigma_{xx} - \sigma_{zz}}{2\sigma_{xz}}\right)^2 + 1} \tag{86}$$

Substitution of the variational mechanics stress state gives

$$\frac{dz}{dx} = \frac{k_m^{(1)}\sigma_0 - \psi(x) - \frac{\psi''(x)}{2}(ht_1 - z^2)}{2\psi'(x)z} + \sqrt{\left(\frac{k_m^{(1)}\sigma_0 - \psi(x) - \frac{\psi''(x)}{2}(ht_1 - z^2)}{2\psi'(x)z}\right)^2 + 1} \tag{87}$$

Numerical integration of Eq. (87) starting at the principle stress maximum on the $90/(S)$ interface gives a prediction of the shape of the curved microcracks. The initial angle and the overall trajectory are a reasonable agreement with experimental observations [85]. Lastly, we indicate that no one has reported curved microcracks in $[90_n/(S)]_s$ laminates.

5.5.   *Individual Microcrack Propagation*

Previous sections discuss micromechanics of damage models for microcracking that assume microcracks form when the energy release rate upon forming a complete microcrack exceeds some critical energy release rate — G_{mc}. This model has its origins in fracture mechanics, but it is unconventional and therefore non-rigorous

fracture mechanics. A more rigorous fracture mechanics approach requires analyzing the growth of individual microcracks as they propagate in the width (y) direction. Individual microcracks initiate at the free edge as partial microcracks that span the thickness of the 90° plies (see Fig. 1). A rigorous fracture mechanics approach to predicting the propagation of such partial microcracks would involve calculating the energy release rate for an infinitesimal amount of partial microcrack growth.

When studying partial microcrack propagation, there are two difficult problems to surmount. First, the stress analysis of partial microcracks requires a three dimensional stress analysis. No one has attempted either approximate analytical three-dimensional stress analysis or finite element analysis of partial microcracks. Hashin [67, 68] presents some three-dimensional, variational mechanics techniques in solving for the stress in $[0_m/90_n]_s$ laminates with microcracks in both the 0° and the 90° plies. His techniques may be applicable to partial microcracks. Three-dimensional finite element analysis of partial microcracks is relatively straight forward and could provide valuable insight into microcrack propagation. The second problem is that most microcracks instantaneously span the entire cross-section of the 90° plies. Because the process of individual microcrack propagation is only observed under unusual circumstances (thin 90° plies [13] and low stress fatigue [21, 35]) microcrack growth theories are difficult to verify experimentally.

There are some qualitative theoretical results for individual microcrack propagation. Both Dvorak and Laws [86, 87] and Hahn and Johannesson [88] claim that the energy release rate for the width (y) direction propagation of a partial microcrack is independent of the length of that microcrack. Their claims, however, are not based on three-dimensional stress analysis of a partial microcrack in a cross-ply laminate. Dvorak and Laws [86, 87] claims are further limited to isolated microcracks or microcrack initiation. Based on qualitative stress trajectories and a two-dimensional stress analysis in isotropic, homogeneous materials [89], Ogin $et.$ $al.$ [45, 46] similarly claim that the stress intensity factor (or energy release rate) for a partial microcrack is independent of its length. They use the one-dimensional analysis that assumes parabolic displacement [45, 46, 64] to estimate the stress intensity factor. They analyze partial microcracks growing in the microcrack interval between two existing complete microcracks and argue that while the stress intensity factor is independent of the length of the partial microcrack, it does depend on the size of the microcrack interval in which it grows. The stress intensity factor is proportional to the square root of the microcrack interval size [45, 46].

Boniface and Ogin [21] attempted to verify a constant stress intensity factor (or energy release rate) using fatigue crack growth experiments. They exploit the experimental observation that during low stress fatigue partial microcracks are observed to slowly propagate across the sample width [21, 35]. They measure partial microcrack length as a function of cycle number for a series of partial microcracks in different size microcrack intervals. The result is that partial microcrack growth rate, da/dN, is constant for a given microcrack interval size. According to the Paris law for fatigue crack propagation [79], the partial microcrack growth rate should be governed by

$$\frac{da}{dN} = A\Delta K^n \tag{88}$$

where ΔK is the range in stress intensity factor during the fatigue cycle and A and n are material properties. The experimental results and Eq. (88) support the claim that the stress intensity factor for a partial microcrack is independent of its length, but a function of the size of the microcrack interval. Due to the inherent scatter of fatigue crack propagation experiments and the empirical nature of the Paris law [79], we view the experimental results as consistent with a constant stress intensity factor but not as compelling evidence that the stress intensity factor is exactly constant. There may be subtle, but important variations in stress intensity factor as the partial microcrack grows across the laminate width, especially at the two edges

The micromechanics of damage analysis of microcracking only considers the energy release rate for the formation of a complete microcrack. If it is true that the energy release rate for the propagation of a partial microcracks is independent of its length, then we can propose an explanation as to why a micromechanics of damage model that uses non-rigorous fracture mechanics agrees well with experimental results. If we define $G_p(l)$ as the energy release rate for a partial microcrack of length l propagating in the width (y) direction, then the energy release rate for the formation of the complete microcrack is

$$G_m = \frac{1}{W}\int_0^W G_p(l)dy \tag{89}$$

Eq. (89) is general, but if $G_p(l)$ is independent of l, it reduces to $G_m = G_p(l)$. In other words, the energy release rate calculated by only considering complete microcracks is the same as the energy release rate for a partial microcrack. We define the rigorous fracture mechanics problem as predicting when the next flaw in the $90°$ plies will become critical and form a complete microcrack. When $G_p(l)$ is independent of flaw size and $G_m = G_p(l)$, the solution to the rigorous fracture mechanics problem is identical to the micromechanics of damage solution that only seeks to predict the formation of complete microcracks. The solutions are identical because the partial microcrack length never enters the expressions.

6.   Conclusion

Many features about microcracking and microcrack induced damage can be predicted using energy release rate failure criteria. The most complete predictions are those that use Hashin's two-dimensional, variational mechanics stress analysis [65, 66], and extend it when necessary to include thermal stresses [69], antisymmetric or staggered microcracks [54], and delaminations [55]. Coupling energy release rate failure criteria with variational mechanics stress analysis thus provides a successful micromechanics of damage model. We conclude by reviewing Eyring's [6] comments about model building:

Models should start out simple and definite enough that predictions are made. The model assumes that fracture occurs when the energy release rate exceeds some critical energy release rate for the material. With this assumption and a two-dimensional, variational mechanics analysis, the model makes predictions about microcrack initiation, microcrack density as a function of applied load, the effect of thermal stresses, the initiation of microcrack induced delaminations, and the appearance of curved microcracks. For the model to be definite or to be able to predict microcracking in any laminate, the critical energy release rate must be a material constant that is independent of laminate structure. Predictions based on a constant critical energy release rate are in good agreement with experimental results. Some alternative models rely on *in situ* parameters such as an *in situ* transverse strength. Such models are indefinite and thus can not produce satisfactory micromechanics of damage models.

A model is of limited value except as it correlates a substantial body of observable material. The microcrack density predictions are substantiated by extensive comparison to experimental results. The experimental verifications include $[0_m/90_n]_s$, $[\pm\theta/90_n]_s$, $[90_n/0_m]_s$, and $[90_n/\pm\theta]$ laminates. The ability to explain results from both $[(S)/90_n]_s$ and $[90_n/(S)]_s$ laminates is a triumph of the two-dimensional, variational mechanics stress analysis. Some alternative models rely on one-dimensional stress analyses. Such models can not correlate the microcracking properties of a wide variety of laminates and thus can not produce satisfactory micromechanics of damage models. Predictions about the effect of thermal stresses, the initiation of microcrack induced delaminations, and the appearance of curved microcracks are less substantiated by comparison to experiments. The problem is that experimental results are scarce and mostly qualitative. The experimental results that are available agree with the model predictions.

Models that suggest new experiments, even if the theory must be modified, can be useful. The microcracking model is not perfect and in some places is incomplete. The micromechanics of damage analysis process, however, helps clarify what new experiments and analytical work should be done. Perhaps the most important problem is the one of individual microcrack propagation. Studying the propagation of partial microcracks can lead to a more fundamental understanding of microcracking based on rigorous fracture mechanics principles and can clarify the role of processing flaws. Another important problem is to understand the imperfections in the model that occur when microcracks grow in thick $90°$ ply groups. These imperfections suggest work on more accurate stress analyses that do not assume the stress is independent of z and additional work on partial microcrack propagation. When the $90°$ plies are thick, the microcrack formation process may be influenced by crack growth in the thickness (z) as well as the width (y) direction [86, 87]. Finally, the ability of microcracks to induce $90/(S)$ interface delaminations needs quantitative experimental work. A possible experiment would be to measure the critical microcrack density for initiation of delamination [55]. Such experiments would either substantiate the model predictions or point to ways the model needs to be modified.

By Eyring's [6] criteria for a successful model, the micromechanics of damage analysis of microcracking and microcrack induced damage is relatively advanced. Some might be tempted to claim that the microcracking problem is well enough understood that we should move on to new problems and to laminates that are technologically more important than $[(S)/90_n]_s$ and $[90_n/(S)]_s$ laminates. We claim that such thinking

is contrary to the overall goal of understanding failure of composite laminates. First, there are many basic issues in microcracking that are not understood or are only poorly understood. Some examples include the initiation of damage at free edges, the propagation of microcracks across the cross-section of the $90°$ plies, the initiation and propagation of delaminations from straight or curved microcracks, longitudinal splitting in adjacent plies, microcrack formation in composite tubes, and microcrack formation in $\theta \neq 90$ plies of laminates with no $90°$ plies. Second, when selecting $[(S)/90_n]_s$ or $[90_n/(S)]_s$ laminates for basic experiments on composite fracture, the technological importance of those laminates should not be a major consideration. The damage process of matrix microcracking followed by delamination and other failure modes is basic to all composite laminates. The choice of studying those processes in $[(S)/90_n]_s$ and $[90_n/(S)]_s$ laminates is to be able to get some basic insight into the micromechanics of damage. If we insist on studying only technologically important laminates without first understanding the basic mechanisms of damage in simpler laminates, our likelihood of success will be very low and the cost will be high.

Acknowledgements

References

1. M. F. Kanninen and C. H. Popelar, *Advanced Fracture Mechanics* (Oxford University Press, New York, 1985).
2. M. L. Williams, *J. Appl. Mech.*, **24**, (1957).
3. R. Talreja, *J. Comp. Mat.*, **19**, 355 (1985).
4. R. Talreja, *Proc. Roy. Soc. London*, **A399**, 355 (1985).
5. R. Talreja, *Eng. Fract. Mech.*, **25**, 751 (1986).
6. H. Eyring, *Ann. Rev. Phys. Chem.*, **28**, 1 (1977).
7. L. J. Broutman and F. J. McGarry, 17th Reinforced Plastics Conference (Society of Plastics Industry, New York, 1962) Section 1E.
8. M. J. Owen and R. Dukes, *J. Strain Anal.*, **2**, 272 (1967).
9. E. Pink, J. D. Campbell, *J. Mat. Sci.*, **9**, 658 (1974).
10. H. T. Hahn and S. W. Tsai, *J. Comp. Mat.*, **8**, 299 (1974).
11. K. W. Garrett and J. E. Bailey, *J. Mat. Sci.*, **12**, 157 (1977).
12. K. W. Garrett and J. E. Bailey, *J. Mat. Sci.*, **12**, 2189 (1977).
13. A. Parvizi, K. W. Garrett, and J. E. Bailey, *J. Mat. Sci.*, **13**, 195 (1978).
14. A. Parvizi and J. E. Bailey, *J. Mat. Sci.*, **13**, 2131 (1978).
15. J. E. Bailey, P. T. Curtis and A. Parvizi, *Proc. R. Soc. Lond. A*, **366**, 599 (1979).
16. M. G. Bader, J. E. Bailey, P. T. Curtis, and A. Parvizi, *Proc. 3rd Int'l Conf. on Mechanical Behavior of Materials*, **3**, 227 (1979).
17. J. E. Bailey and A. Parvizi, *J. Mat. Sci.*, **16**, 649 (1981).
18. F. R. Jones, A. R. Wheatley, and J. E. Bailey, in *Composite Structures* (*ed.* I. H. Marshall, Appl. Sci. Publ, Barking, 1981), 415.
19. D. L. Flaggs and M. H. Kural, *J. Comp. Mat.*, **16**, 103 (1982).
20. P. W. Manders, T. W. Chou, F. R. Jones, and J. W. Rock, *J. Mat. Sci.*, **19**, 2876 (1983).
21. L. Boniface and S. L. Ogin, *J. Comp. Mat.*, **23**, 735 (1989).
22. A. L. Highsmith and K. L. Reifsnider, *ASTM STP*, **775**, 103 (1982).
23. M. G. Bader and L. Boniface, *Proc. 5th Int'l Conf. on Comp. Mat.*, , 221 (1985).
24. M. Caslini, C. Zanotti, and T. K. O'Brien, *J. Comp. Tech. & Res.*, **Winter**, 121 (1987). (Also appeared as NASA TM89007, 1986).
25. A. S. D. Wang, P. C. Chou and S. C. Lei, *J. Comp. Mat.*, **18**, 239 (1984).

26. A. S. D. Wang, *Comp. Tech. Rev.*, **6**, 45 (1984).

27. A. S. D. Wang, N. N. Kishore and C. A. Li, *Comp. Sci. & Tech.*, **24**, 1 (1985).

28. A. S. D. Wang, *Naval Air Development Center Report No. NADC 85118-60* (1985).

29. S. Liu and J. A Nairn, *J. Reinf. Plast. and Comp.*, **11**, 158 (1992).

30. S. Yalvac, L. D. Yats, and D. G. Wetters, *J. Comp. Mat.*, **25**, 1653 (1991).

31. J. A. Nairn, S. Hu, S. Liu, and J. Bark, *Proc. of the 1st NASA Advanced Comp. Tech. Conf.*, Seattle, WA, Oct. 29 to Nov. 1, 1990.

32. J. A. Nairn, S. Hu and J. Bark, *J. Mat. Sci.*, **28**, 5099 (1993).

33. K. C. Jen and C. T. Sun, *Proc. of the Amer. Soc. Comp, 5th Tech. Conf.*, p. 350 (1990).

34. P. W. M. Peters, *J. Comp. Mat.*, **18**, 545 (1984).

35. L. Boniface, P. A. Smith, S. L. Ogin, and M. G. Bader, *Proc. 6th Int'l Conf. on Comp. Mat.*, **3**, 156 (1987).

36. R. Jamison, K. Schulte, K. L. Reifsnider, and W. W. Stinchcomb, *ASTM STP*, **836**, 21 (1984).

37. S. E. Groves, C. E. Harris, A. L. Highsmith, and R. G. Norvell, *Experimental Mechanics*, **March**, 73 (1987).

38. S. Yalvac, L. D. Yats, and D. G. Wetters, 8th *Int'l Conf. on Comp. Mat.*, 38-J (1991).

39. K. L Reifsnider, *Proc. 14th Ann. Mtg of SES*, Lehigh, PA, November, 1977.

40. F. W. Crossman, W. J. Warren, A. S. D. Wang, and G. E. Law, Jr., *J. Comp. Mat. Supplement*, **14**, 88 (1980).

41. A. S. D. Wang, *Proc. 3rd Int'l Conf. on Comp. Mat.*, p. 170 (1980).

42. F. W. Crossman and A. S. D. Wang, *ASTM STP*, **775**, 118 (1982).

43. W. W. Stinchcomb, K. L. Refisnider, P. Yeung, and J. Masters, *ASTM STP*, **723**, 64 (1981).

44. S. Liu and J. A. Nairn, *Proc. of the Amer. Soc. Comp, 5th Tech. Conf.*, p. 287 (1977).

45. S. L. Ogin, P. A. Smith, and P. W. R. Beaumont, *Comp. Sci. & Tech.*, **22**, 23 (1985).

46. S. L. Ogin, P. A. Smith, and P. W. R. Beaumont, *Comp. Sci. & Tech*, **24**, 47 (1985).

47. D. S. Adams, D. E. Bowles, and C. T. Herakovich, *J. Reinf. Plast. and Comp.*, **5**, 152 (1986).

48. R. G. Spain, *Composites*, **2**, 33 (1971).

49. C. T. Herakovich, J. G. Davis, Jr., and J. S. Mills, in *Thermal Stresses in Severe Environments*, (editors: D. P. H. Hasselman and R. A. Heller, Plenum Press, 1980) 649.

50. C. T. Herakovich and M. W. Hyer, *Eng. Fract. Mech.*, **25**, 779 (1986).

51. S. A. Salpekar and T. K. O'Brien, *Proc. 8th Int'l Conf. on Comp. Mat.*, 28-G (1991).

52. D. S. Adams and C. T. Herakovich, *J. Thermal Stresses*, **7**, 91 (1984).

53. D. E. Bowles, *J. Comp. Mat.*, **17**, 173 (1984).

54. J. A. Nairn and S. Hu, *Eng. Fract. Mech.*, **41**, 203 (1992).

55. J. A. Nairn and S. Hu, *Int. J. Fract.*, **57**, 1 (1992).

56. D. L. Flaggs, *J. Comp. Mat.*, **19**, 29 (1985).

57. H. Fukunaga, T. W. Chou, P. W. M. Peters, and K. Schulte, *J. Comp. Mat.*, **18**, 339 (1984).

58. Y. M. Han, H. T. Hahn, and R. B. Croman, *Proc. of the Amer. Soc. Comp, 2nd Tech. Conf.*, p. 503 (1987).

59. Y. M. Han, H. T. Hahn, and R. B. Croman, *Comp. Sci. & Tech.*, **31**, 165 (1987).

60. N. Laws and G. J. Dvorak, *J. Comp. Mat.*, **22**, 900 (1988).

61. R. J. Nuismer and S. C. Tan, *J. Comp. Mat.*, **22**, 306 (1988).

62. S. C. Tan and R. J. Nuismer, *J. Comp. Mat.*, **23**, 1029 (1989).

63. Y. Korczynsky and J. G. Morley, *J. Mat. Sci.*, **16**, 1785 (1981).

64. S. L. Ogin, P. A. Smith, and P. W. R. Beaumont, *Cambridge University Engineering Dept. Tech. Report, CUED/C/MATS/TR.105* (1984).

65. Z. Hashin, *Mechanics of Materials*, **4**, 121 (1985).

66. Z. Hashin, *Eng. Fract. Mech.*, **25**, 771 (1986).

67. Z. Hashin, *J. Appl. Mech.*, **54**, 872 (1987).

68. Z. Hashin, *Comp. Sci. & Tech.*, **31**, 247 (1988).

69. J. A. Nairn, *J. Comp. Mat.*, **23**, 1106 (1989). Errata: *J. Comp. Mat.*, **24**, 233 (1990).

70. G. P. Fang, R. A. Schapery, and Y. Weitsman, *Eng. Fract. Mech.*, **33**, 619 (1989).

71. A. S. D. Wang and R. W. Crossman, *J. Comp. Mat. Supplement*, **14**, 71 (1980).

72. S. A. Salpekar and T. K. O'Brien, NASA TM 102591 (1990).

73. J.C. Fish and S. W. Lee, *ASTM STP*, **1059**, 271 (1990).

74. H. Fukunaga, T. W. Chou, K. Schulte, and P. W. M. Peters, *J. Mat. Sci.*, **19**, 3546 (1984).

75. J. A. Nairn, *Proc. of the Amer. Soc. Comp, 3rd Tech. Conf.*, p. 472 (1988). Relevant Errata: *J. Comp. Mat.*, **24**, 233 (1990).

76. J. A. Nairn, S. Liu, H. Chen, and A. R. Wedgewood, *J. Comp. Mat.*, **25**, 1085 (1991).

77. D. L. Hunston, *Comp. Tech. Rev.*, **6**, 176 (1984).

78. J. A. Barnes, private communication (1991).

79. P. Paris and F. Erdogan, *J. Bas. Eng. Trans. ASME, Ser. D*, **85**, 528 (1963).

80. S. Liu and J. A. Nairn, unpublished results (1991).

81. T. K. O'Brien, *ASTM STP*, **876**, 282 (1985).

82. T. K. O'Brien, *ASTM STP*, **1059**, 7 (1990).

83. L. R. Dharani and H. Tang, *Int'l J. Fracture*, **46**, 123 (1990).

84. S. Hu and J. A. Nairn, unpublished results (1991).

85. S. Hu and J. A. Nairn, *Comp. Sci. & Tech.*, **47**, 321 (1992).

86. G. J. Dvorak and N. Laws, *Fracture of Fibrous Composites*, **AMD-Vol 74, ASME**, 59 (1985).

87. G. J. Dvorak and N. Laws, *J. Comp. Mat.*, **21**, 309 (1987).

88. H. T. Hahn and T. Johannesson, in *Mechanics of Composites*, (AMD-V58, ASME, Editor: G. Dvorak, 1983) 135.

89. M. Isida, *Int. J. Fract. Mech.*, **7**, 301 (1971).